Ductile deformation and mass loss in the Franciscan Subduction Complex: implications for exhumation processes in accretionary wedges

UWE RING[1] & MARK T. BRANDON[2]

[1]*Institut für Geowissenschaften, Johannes Gutenberg-Universität, Becherweg 21, 55099 Mainz, Germany (e-mail: ring@mail.uni-mainz.de)*

[2]*Kline Geology Laboratory, Yale University, P.O. Box 208109, New Haven, CT 06520–8109, USA*

Abstract: Deformation measurements from 64 sandstone samples collected in three study areas from the Eastern Belt of the Franciscan Complex are used to evaluate how the high-pressure metamorphic interior of the Franciscan wedge was exhumed. Pressure estimates indicate 25–30 km of exhumation in this part of the Franciscan Complex. Much of the Eastern Belt has a semi-penetrative cleavage that formed by solution mass transfer (SMT) while the rocks were moving through the wedge. Individual samples have absolute principal stretches of S_X = 1.00–1.52, S_Y = 0.60–1.21, and S_Z = 0.33–0.81. Strain magnitudes and directions are quite variable at the local scale. The deformation at the regional scale is estimated by calculating tensor averages for groups of measurements. The three study areas, which are spaced over a distance of *c.* 500 km along the Franciscan margin, give remarkably similar averages, which indicates that the deformation of the Eastern Belt is consistent at the regional scale. The tensor average for all data indicates a nearly vertical Z direction with S_X = 0.96, S_Y = 0.92, and S_Z = 0.70. S_X and S_Y are near one because at the local scale, the X and Y directions vary considerably in orientation, which means that their stretch contributions are averaged out at the regional scale. This unusual strain type, consisting of both plane strain and uniaxial shortening, results from the fact that shortening in Z was balanced by a pervasive mass-loss volume strain, averaging about 38%. The geometry of directed fibre overgrowths was used to measure internal rotations. These data indicate that in sandstones, SMT deformation was nearly coaxial (mean kinematic vorticity number is 0.05 at the regional scale and generally <0.4 for individual samples). A simple one-dimensional steady-state model indicates that ductile thinning accounted for only *c.* 10% of the overall exhumation. Ductile shortening across the Franciscan wedge was very slow, at rates $<8 \times 10^{-17}$ s^{-1} (<0.3% Ma^{-1}). Assuming that this strain was active in an across-strike zone <200 km wide, we estimate that horizontal ductile flow would have accounted for <0.25% of the total convergence across the Franciscan margin. We conclude that the SMT mechanism operated slowly as a background deformation process, and that the dislocation glide mechanism was completely inactive down to depths of 25–30 km. Thus, the stability of the Franciscan wedge was probably better defined by the Coulomb wedge criterion than by a viscous wedge criterion. No definitive normal faults have been found in or adjacent to the Eastern Belt. Therefore, we infer that wedge taper was mainly controlled by deep accretion and erosion of an emergent forearc high.

A fundamental problem in tectonics is the cause of deep exhumation of high-pressure metamorphic rocks commonly found in the interior of many convergent wedges. In recent years, extensional faulting has received considerable attention because it provides an elegant and possibly widely applicable mechanism for unroofing a wedge (e.g. Platt 1986, 1993; Dewey 1988). In addition to normal faulting, erosion (e.g. England & Richardson 1977; Rubie 1984; Brandon *et al.* 1998) and syn-convergent ductile flow (e.g. Selverstone 1985; Wallis 1992; Wallis *et al.* 1993; Feehan & Brandon 1999) can also contribute to exhumation of a convergent wedge.

Three different settings of deep exhumation have been recognized. One is in the internal zones of continent–continent collisions where exhumed high-pressure metamorphic rocks, including both high-temperature and low-temperature varieties, are found. This setting contains some of the deepest exhumed rocks, coesite- and diamond-bearing rocks coming from depths >100 km (e.g. Chopin 1984; Coleman & Wang 1995).

A second setting is found in ancient subduction complexes and is characterized by exotic blocks of blueschist and eclogite immersed in a matrix of highly deformed mudstone or

RING, U. & BRANDON, M. T. 1999. Ductile deformation and mass loss in the Franciscan Subduction Complex: Implications for exhumation processes in accretionary wedges. *In:* RING, U., BRANDON, M. T., LISTER, G. S. & WILLETT, S. D. (eds) *Exhumation Processes: Normal Faulting, Ductile Flow and Erosion*. Geological Society, London, Special Publications, **154,** 55–86.

serpentinite. These blocks typically come from depths of 30–60 km. A classic example of this setting is the knocker terrane of the Central Belt of the Franciscan Complex. The process of exhumation remains poorly understood. Platt (1986) favoured normal faulting, whereas Cloos & Shreve (1988) proposed upward transport by deep-seated channelized flow at the base of the wedge.

We focus here on a third setting, where large coherent tracts of low-temperature–high-pressure metamorphic rocks have been exhumed in subduction-related accretionary wedges. The metamorphic rocks involved are typically of prehnite–pumpellyite, lawsonite–albite, pumpellyite–actinolite, blueschist, or more rarely greenschist facies. The coherence of these terranes is indicated by the common preservation of metamorphic isograds within the terranes. The depth of exhumation is usually no greater than about 35 km, which is consistent with the maximum thickness of modern subduction-related wedges. Normal faulting is often cited as a likely exhumation process in this setting. The island of Crete, which marks the modern forearc high of the Hellenic convergent margin, provides an example of syn-convergent normal faulting (Fassoulas *et al.* 1994; Thomson *et al.* this volume). Normal faulting there seems to be controlled by roll-back of the Hellenic subduction zone. Platt (1986, 1987), Jayko *et al.* (1987), and Harms *et al.* (1992) have argued that coherent low-temperature–high-pressure metamorphic terranes in the Eastern Belt of the Franciscan Complex were unroofed by syn-convergent normal faulting. In contrast, erosion appears to be the primary exhumation process for the modern forearc high at the Cascadia margin (Brandon *et al.* 1998).

In this paper, we report new deformation measurements from the coherent metamorphic terranes of the Eastern Belt of the Franciscan Complex and use this information to resolve the deformation field that existed within the Franciscan wedge. The high-pressure metamorphic rocks of the Eastern Belt show extensive evidence of solution mass transfer (SMT) deformation. The clockwise *P–T* loop for these rocks indicates a general displacement path involving subduction, then accretion at the base of the wedge, upward flow within the wedge, followed by exhumation and exposure at the Earth's surface. We maintain that these deeply exhumed rocks provide a path-integrated record of the deformation-rate field in the wedge. We utilize some new methods, which provide a full determination of the absolute finite deformation produced by the SMT mechanism, including volume strain and internal rotation. These methods are the projected dimension strain (PDS) method, the mode method and the semi-deformable antitaxial (SDA) fibre method. The contribution of vertical ductile thinning to exhumation is estimated using a simple one-dimensional steady-state model by Feehan & Brandon (1999). The data reported herein, combined with our work on the kinematic evolution of the Coast Range fault zone (Ring & Brandon 1994, 1997), allow us to approximate the relative contributions of different processes to the total exhumation of the Eastern Belt metamorphic rocks.

Overview

Geological and tectonic setting

The Franciscan Complex represents a long-lived accretionary wedge, Late Jurassic to Paleogene in age, which grew along the western edge of the North American Cordillera (Fig. 1a). This convergent margin is preserved in three northwest-trending tectonic zones: the Franciscan Complex was the subduction complex or accretionary wedge, the Sierra Nevada batholith was the magmatic arc, and the Great Valley basin formed between these as a broad forearc basin (e.g. Ingersoll 1978, 1979; Blake *et al.* 1988; Cowan & Bruhn 1992). The basement to the forearc is a Jurassic ophiolite, called the Coast Range ophiolite. At present, the Franciscan Complex is separated from the Coast Range ophiolite and overlying Upper Jurassic and Cretaceous strata of the Great Valley basin by the Coast Range fault zone. Platt (1986) called attention to the strong break in metamorphic grade across the Coast Range fault. The Coast Range ophiolite and the lowermost units of the Great Valley sequence show zeolite- to incipient prehnite–pumpellyite-facies metamorphism (Dickinson *et al.* 1969), whereas west of the fault, the Eastern Belt of the Franciscan Complex records blueschist-facies metamorphism (Fig. 1b).

The Franciscan Complex is dominated by clastic sedimentary rocks, interpreted as accreted trench sediments and superimposed trench-slope basins. It also includes subordinate mafic and keratophyric volcanic rocks and thick chert sequences, which represent, at least in part, accreted fragments of seamounts and oceanic plateaux, as well as imbricated slices from the overlying Coast Range ophiolite. In the northern Coast Range, the Franciscan Complex is commonly subdivided into three northwest-trending belts (Fig. 1a), which are, from west to east: the Coastal, Central and Eastern Belts

(Bailey *et al.* 1964; Berkland *et al.* 1972; Blake *et al.* 1988). Stratigraphic age, as well as the degree and age of metamorphism and deformation, generally increase to the east across these belts. South of San Francisco, this subdivision is not as apparent, probably because of disruption by young faulting associated with the modern San Andreas transform boundary.

We focus on the Eastern Belt, which constitutes the uppermost part of the Franciscan Complex (Fig. 1b). The term Eastern Belt refers to a gently east-dipping sequence of nappe-like units, each of which contains a relatively coherent internal stratigraphy (Suppe 1973; Cowan 1974; Worrall 1981; Blake *et al.* 1988; Jayko & Blake 1989). The faults that bound these units appear to be everywhere post-metamorphic (Suppe 1973; Cowan 1974; Platt 1975; Worrall 1981). Metamorphic grade is generally lawsonite–albite or blueschist facies as indicated by the presence of widespread lawsonite and aragonite, and more localized glaucophane and jadeite (e.g. Worrall 1981; Blake *et al.* 1988; Ernst 1993). The two main units within this structural succession are the Yolla Bolly terrane and the structurally higher Pickett Peak terrane (Blake *et al.* 1988; Fig. 1). The Pickett Peak terrane, which is restricted to the northern Coast Range, contains two structural units: the South Fork Mountain Schist and the underlying Valentine Springs Formation (Worrall 1981). Maximum temperatures were about 400°C in the South Fork Mountain Schist, and between 250°C and slightly greater than 310°C in the Valentine Springs Formation (Jayko *et al.* 1986; Blake *et al.* 1988; Tagami & Dumitru 1996). Maximum metamorphic pressures for both units were in the range 6–9 kbar (23–34 km depth assuming an average density of 2700 kg m^{-3}) (Blake *et al.* 1988). The Yolla Bolly terrane experienced lower metamorphic conditions, 125–200°C and 6–8 kbar (23–30 km) in the Yolla Bolly Mountains (Jayko *et al.* 1986; Bröcker & Day 1995), and 100–200°C and 7 to >8 kbar (26 to >30 km) in the Pacheco Pass area of the Diablo Range (Ernst 1993).

Isotopic ages from the Eastern Belt indicate a protracted history of high-pressure metamorphism, followed by slow cooling in Late Cretaceous and early Cenozoic time (Suppe & Armstrong 1972; Lanphere *et al.* 1978; McDowell *et al.* 1984; Mattinson 1988; Dumitru 1989; Wakabayashi 1992; Tagami & Dumitru 1996). The oldest metamorphic ages of 150–165 Ma are from high-grade blueschist-, eclogite- and amphibolite-facies blocks (K–Ar ages on phengite and hornblende, Rb–Sr mineral ages on aragonite/glaucophane and phengite–zoisite pairs, and a U–Pb isochron age for glaucophane, lawsonite and sphene; Coleman & Lanphere 1971; Nelson & DePaolo 1985; Mattinson 1988). As for the Pickett Peak terrane, its stratigraphic age remains poorly known, but regional high-pressure metamorphism is thought to have occurred at about 125–130 Ma (Ar–Ar whole-rock ages, Lanphere *et al.* 1978). The upper part of the Yolla Bolly terrane has yielded rare Berriasian to Valanginian fossils, indicating deposition sometime during 138–119 Ma. Regional metamorphism of this part of the Yolla Bolly terrane occurred at about 115–120 Ma (Rb–Sr whole-rock isochron, Peterman *et al.* 1967; U–Pb isochron on garnet, amphibole, and sphene, Mattinson 1986; Ar–Ar on hornblende, Weinrich *et al.* 1997). However, lawsonite- and aragonite-bearing shale and sandstone from the lower part of the Yolla Bolly terrane have yielded Cenomanian (97–91 Ma) *Inocerami* (Hull Mountain area in northern California, Blake *et al.* 1988). Metamorphism of this part of the Yolla Bolly terrane is younger as well, as indicated by U–Pb isotopic ages on sphene and plagioclase from a metamorphosed gabbro intrusion indicating peak metamorphism at 92 Ma (Ortigalita Peak gabbro in the Diablo Range, Mattinson & Echevirra 1980). We concur with others (e.g. Mattinson 1988; Wakabayashi 1992) that the range of metamorphic ages is probably related to protracted accretion and high-pressure metamorphism, but this interpretation remains difficult to prove.

A variety of evidence indicates that the Eastern Belt was mainly exhumed during Late Cretaceous and early Cenozoic time (Krueger & Jones 1989). In central California, Upper Cretaceous (Campanian?) trench-slope basins received blueschist and chert clasts derived from an uplifted Franciscan-like source (Cowan & Page 1975; Smith *et al.* 1979). Parts of the Great Valley basin itself became shallow and locally emergent during Late Cretaceous and early Tertiary time (Ingersoll 1978, 1979; Dickinson *et al.* 1982). Berkland (1973) recognized Paleocene (66–55 Ma) conglomerates in the northern Coast Ranges that contained abundant Franciscan detritus including clasts of lawsonite- and pumpellyite-bearing metagreywacke, which Berkland (1973) noted as 'indistinguishable in texture and mineralogy from the bedrock of the Eastern Belt of the Franciscan Complex'. In the central Coast Ranges, the first Franciscan detritus appears in the Lower Eocene deposits (*c.* 53 Ma, Domengine Formation; Moxon 1988). Page & Tabor (1967) and Pampeyan (1993) described a pre-Middle Eocene unconformity cut into the Franciscan Complex south of San Francisco.

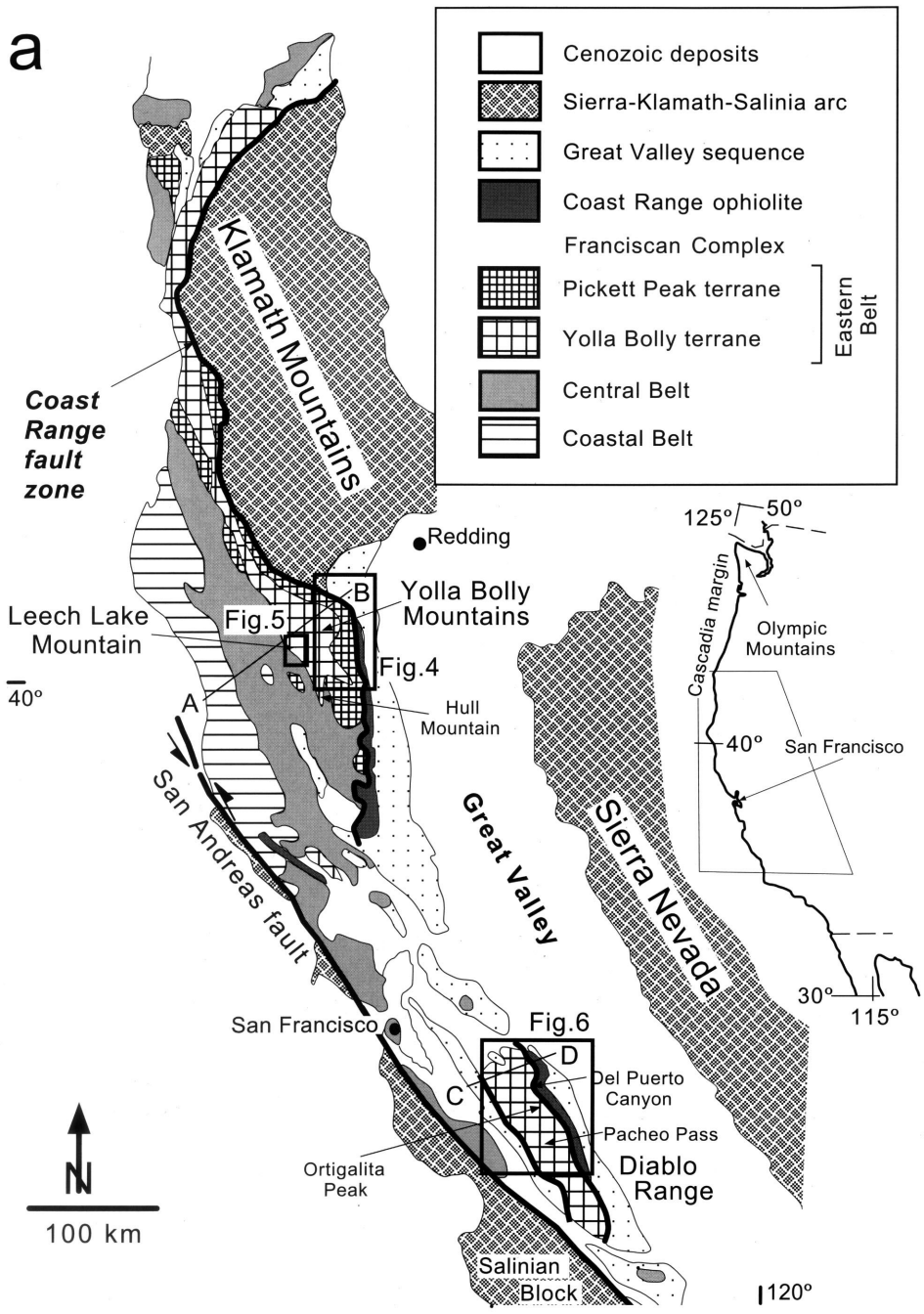

Fig. 1. (**a**) Geological map showing Mesozoic tectonic features of western California. The smaller inset map shows the location of the geological map relative to the coast of western North American. Our three study areas are located in the Yolla Bolly Mountains (Fig. 4) and at Leech Lake Mountain (Fig. 5) in northern California and in the Diablo Range (Fig. 6) of central California. Also shown are localities referred to in the text. (**b**) Generalized cross-section through the Yolla Bolly Mountains (A–B, after Cowan & Bruhn 1992) and the northern Diablo Range (C–D, after Bauder & Liou 1979).

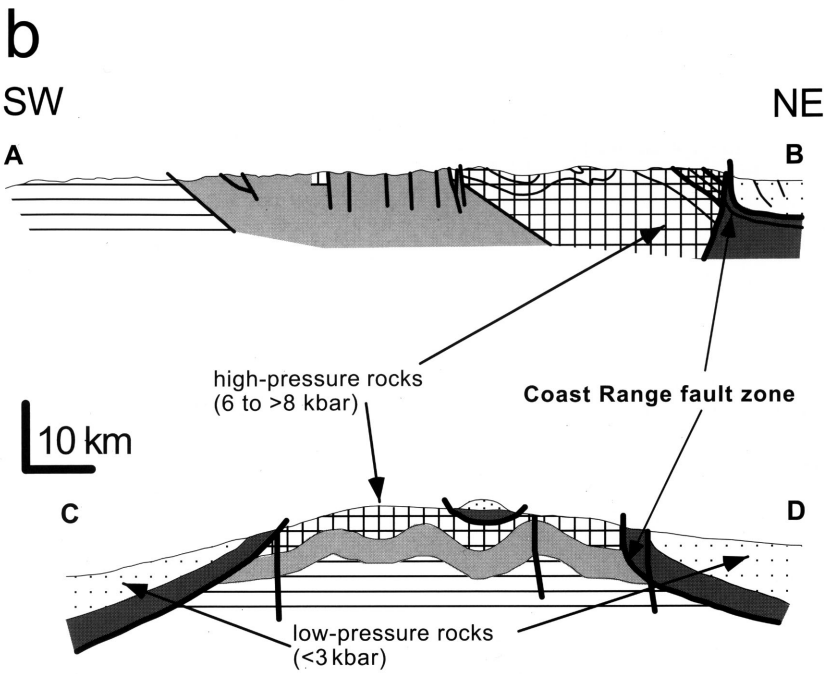

This sedimentological evidence is consistent with zircon and apatite fission-track ages by Dumitru (1989) and Tagami & Dumitru (1996) that indicate slow cooling during the Late Cretaceous and early Cenozoic time.

Residence time and average exhumation rates

The timing information given above is used here to estimate wedge residence times and exhumation rates for our study areas in the Eastern Belt (Table 1). First, we assume that the age of accretion is closely approximated by the age of peak metamorphism. To illustrate, let us consider an average accretionary wedge with a surface slope *c.* 3° and basal décollement dipping at *c.* 5° (Davis *et al.* 1983). Seven kilometres of convergence are needed to obtain 1 km of structural burial. Convergence rates at the Franciscan margin were *c.* 100 km Ma^{-1} in Late Cretaceous time (Engebretson *et al.* 1985). Thus, subduction to a depth of *c.*25–30 km would have taken less than *c.* 2 Ma. Peak metamorphism should have followed rapidly after accretion to the base of the wedge. We infer from sedimentological data and apatite fission-track ages that Eastern Belt rocks exposed at present in our study areas were at or near the surface by *c.* 60 Ma.

The wedge residence time for our northern

Table 1. *Orogenic parameters for Eastern Belt of the Franciscan Complex*

Unit and study area	Depth of accretion (km)	Residence time (Ma)
Valentine Springs Fm, Yolla Bolly Mtns	23–34	65–70
Yolla Bolly terrane, Yolla Bolly Mtns and Leech Lake Mtn	23–30	55–60
Yolla Bolly terrane, Diablo Range	26–>30	32–37

California study areas in the Yolla Bolly Mountains and Leech Lake Mountain is estimated to about 65–70 Ma for the Valentine Springs Formation and 55–60 Ma for the upper part of the Yolla Bolly terrane. The Eastern Belt rocks in our Diablo Range study area are probably correlative with the lower part of the Yolla Bolly terrane. The 92 Ma metamorphic age for the Ortigalita Peak gabbro indicates a residence time of about 32–37 Ma for these rocks. These estimates are crude but should be accurate to within ±20%. Based on metamorphic depths and residence times, we estimate that exhumation rates were about 0.3–0.5 km Ma^{-1} for the Valentine Springs Formation and Yolla Bolly terrane in the northern California study areas, and 0.7–0.9 km Ma^{-1} for the Yolla Bolly terrane in the Diablo Range study area.

Exhumation of Franciscan high-pressure rocks

Platt (1986) proposed the provocative idea that normal slip on the Coast Range fault zone was responsible for exhumation of the high-pressure metamorphic interior of the Franciscan wedge. He argued that underplating could drive a viscous convergent wedge into a supercritical taper where the upper part of the wedge would start to flow or fail by horizontal extension. Jayko *et al.* (1987) and Harms *et al.* (1992) provided additional evidence for normal slip on the Coast Range fault zone. Krueger & Jones (1989) and Wakabayashi & Unruh (1995) considered how tectonic exhumation might relate to the accretionary history of the Franciscan margin. We note that the Coast Range fault zone is the only structure to be considered for tectonic exhumation of the high-pressure Eastern Belt rocks. To our knowledge, no other exhumational structures have been recognized or proposed.

Most workers agree that the Franciscan and Coast Range Ophiolite were originally separated by a subduction-related thrust fault. This hypothetical structure would probably have been formed during the initiation of the Franciscan subduction zone, but such an early structure has never been definitively identified. Platt (1986), Jayko *et al.* (1987), and Harms *et al.* (1992) made the important point that much of the Coast Range fault zone was formed late relative to the initiation of the Franciscan subduction zone. Their arguments in favour of the normal fault interpretation were: (1) the Coast Range fault cuts out metamorphic section between high-pressure Franciscan metamorphic rocks and the very low-grade rocks of the Great Valley forearc basin and Coast Range ophiolite (Fig. 1b) (Platt 1986); (2) the Coast Range ophiolite, which lies above and within the Coast Range fault zone, appears to have been thinned by Coast Range faulting (Platt 1986; Jayko *et al.* 1987); (3) kinematic indicators from Franciscan rocks beneath the Del Puerto segment of the Coast Range ophiolite (Fig. 1) were used to infer top-east normal slip on the Coast Range fault zone (Harms *et al.* 1992).

We maintain that the first two arguments are inconclusive because out-of-sequence thrusting can also result in younger-over-older relationships and can attenuate metamorphic and stratigraphic sections. This will happen when contractional faults cut through a section that dips steeply in a direction opposite the hanging-wall transport direction (Ring & Brandon 1994; Wheeler & Butler 1994; Ring 1995). Kinematic data from the Coast Range fault zone (Ring & Brandon, 1994, 1997) indicate east-side-up motion, which is not compatible with the normal-slip interpretation. These data have been interpreted by Ring & Brandon (1994, 1997) to indicate that the Coast Range fault formed as a post-metamorphic, out-of-sequence thrust with a generally east-side-up or top-west sense of motion. We have already noted above that the Yolla Bolly and Pickett Peak terranes are cut by a series of widely spaced east-dipping faults, all of which appear to be post-metamorphic. Thus, these intra-Franciscan faults may have thickened the original metamorphic section by placing high-grade over low-grade rocks.

As noted above, Harms *et al.* (1992) used asymmetric fabrics in Eastern Belt sandstones to infer top-east shearing on the Coast Range fault zone at Del Puerto Canyon. The Del Puerto area is important because it may preserve a relative old segment of the fault zone, unaffected by Cenozoic tectonic wedging (Harms *et al.* 1992). Our measurements from Del Puerto indicate nearly coaxial deformation in the Eastern Belt, and thus are inconsistent with the ductile shearing interpretation of Harms *et al.* (1992). We return to this issue in the Discussion section.

We envision that many of the post-metamorphic faults in and adjacent to the Franciscan Complex are related to Cenozoic shortening across the Coast Range. The tectonic wedging models of Wentworth *et al.* (1984) and Unruh *et al.* (1995) have called attention to this young deformation but they do not address in any detail the possibility of young slip on the intra-Franciscan post-metamorphic faults. The point to be stressed is that, at present, there are no structures within the Great Valley–Franciscan boundary that can be equated to the normal faults predicted by Platt's (1986) model. The

Franciscan Complex might have been exhumed by normal faulting, but there is no longer any direct evidence for such structures.

Platt (1986) based his model for exhumation of the Eastern Belt on the critical-wedge concept as originally outlined by Chapple (1978) and Davis *et al.* (1983). Platt (1986) argued that the dominant ductile deformation mechanism within a subduction-related accretionary wedge is SMT, a linear viscous mechanism that operates by selective dissolution and precipitation along grain boundaries. In Platt's model, deep accretion and within-wedge ductile deformation would cause upward flow within the rear of the wedge, resulting in extensional failure in the upper part of the wedge (Platt 1986, 1987). An essential assumption is that within-wedge ductile flow was fast enough to influence the overall stability of the wedge. Platt's model does not provide specific quantitative predictions of strain rate, but he envisioned that ductile strain rates of 10^{-14} s^{-1} (31% Ma^{-1}) or more would be required to destabilize the wedge (Platt, 1986, p. 1040). The model highlights the importance of within-wedge deformation for understanding wedge stability, but there have been surprisingly few quantitative studies of the magnitude, pattern, rate and nature of ductile strain in subduction complexes. Notable exceptions are the studies by Paterson & Sample (1988), Ring *et al.* (1989), Norris & Bishop (1990), Fisher & Byrne (1992), Wallis (1992), and Feehan & Brandon (1999).

SMT deformation in the Franciscan wedge

Petrographic evidence clearly indicates that SMT was the dominant deformation mechanism operating in our sandstone samples. The sandstones are composed of first-cycle volcanic and plutonic detritus. Monocrystalline grains of volcanic quartz and plagioclase show little to no undulose extinction, deformation laminae, or deformation twinning. Polycrystalline quartz grains do show evidence of undulose extinction, but these may have been eroded from metamorphic source rocks. Quartz *c*-axis fabrics from six samples show no preferred crystallographic orientation (Ring 1996). Grain breakage is relatively uncommon. These collective observations are consistent with estimated metamorphic temperatures (see above) that were almost everywhere below the threshold needed to activate dislocation mechanisms in quartz (>300°C, e.g. Küster & Stöckhert 1997).

Quartz, and to a lesser degree feldspar, are truncated by thin selvages composed of insoluble minerals (Fig. 2). Microprobe work reveals that these selvages contain high concentrations of Fe-oxides, rutile, sphene, phengite, and chlorite (Ring 1996). The selvages can be regarded as planes of finite flattening that formed perpendicular to *Z* (Ramsay & Huber 1983). *X*, *Y* and *Z* correspond to the principal strain directions for minimum, intermediate, and maximum shortening, respectively. Directed fibre overgrowths mantle those grain boundaries that lie at a high angle to the trace of cleavage (Fig. 2). Cathodoluminescence work by Ring (1996) indicates that all overgrowths on quartz grains have a directed fibre habit. These fibres are considered to record the entire extensional history of SMT deformation. The overgrowths are generally subparallel to the orientation of the selvages in *XZ* sections (Fig. 2) indicating that the bulk deformation was close to coaxial.

As discussed by Feehan & Brandon (1999), the formation of a SMT fabric requires small offsets between grains on surfaces parallel to the cleavage selvages. The reason is that extension is accommodated in a heterogeneous fashion at the local scale because the sites of fibre growth are not coordinated with each other. The intergranular offsets must be small and discontinuous because the selvages typically are short in length (no more than a couple of grain dimensions) and anastomosing in form. This argument also indicates that during SMT deformation, intergranular slip typically does not occur on surfaces oblique to the selvages. If it did, we would see offsets and distortions of the selvages.

Textural evidence suggests that the sandstones had very little porosity at the start of SMT deformation. All of the space between grains is now occupied by selvages or directed fibre overgrowth. We have found no evidence for isotropic overgrowths. Displacement-controlled fibre overgrowths are thought to form only where the aperture for fibre growth was never greater than several microns (Urai *et al.* 1991; Fisher & Brantley 1992). Some pore space could have been removed where selvages have formed but there is no reason to suspect that the selvage sites had unusual large pore spaces given that the overgrowth sites show no evidence of significant original pore space. Mechanical compaction is characterized by slip on intergranular surfaces of all orientations to accommodate the motion of grains into intervening pore spaces. We have already noted that the parallelism of fibres and selvages indicates that oblique intergranular slip generally did not occur during SMT deformation. Therefore, we conclude that mechanical compaction had already removed much of the primary porosity before the onset of SMT deformation. This result is not unexpected

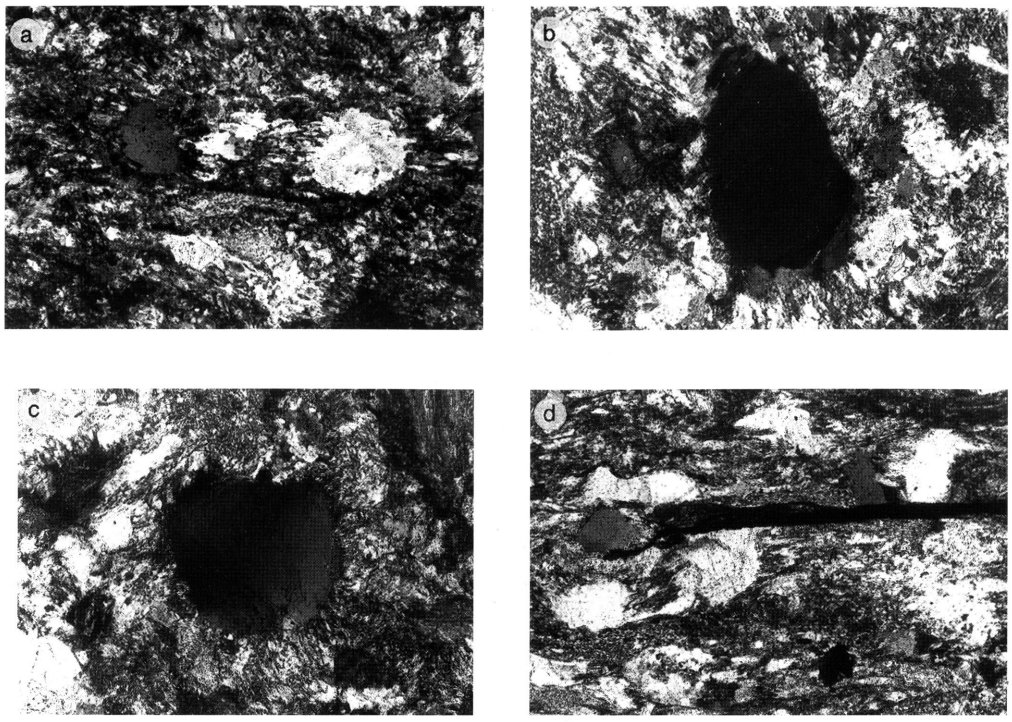

Fig. 2. Typical (**a**) *XZ* and (**b**) *XY* sections from Yolla Bolly sandstones. (**c**) Multidirectional fibres in a *XY* section indicating extension in both *X* and *Y*. (**d**) Overall parallelism between fibrous overgrowth and selvages in *XZ* section indicating little to no internal rotation. Long side of each photograph represents 1.4 mm for (**a**) and (**d**), and 0.8 mm for (**b**) and (**c**); all photomicrographs are in crossed-polarized light. *X* is horizontal in (**a**) and (**d**) and nearly vertical in (**b**).

for poorly sorted sands where grains of different sizes can move together into a tightly packed aggregate.

Relative timing of SMT deformation and metamorphism

Ernst (1965, 1987, 1993) has published detailed textural observations for metamorphic minerals in Eastern Belt sandstones of the Diablo Range. He described host grains of plagioclase and quartz that were replaced by coarsely crystalline prisms of jadeite with concentric and oscillatory zoning. Tiny fibres of jadeite were observed extending from larger jadeite grains into the sandstone matrix. The fibres possessed the same chemical composition as the jadeite host (Ernst 1992). Euhedral jadeite and aragonite were found in quartzose veins as well. Sodic amphibole was observed in stringers and fracture-related patches.

Microprobe analyses (Ring 1996) of samples from Pacheco Pass indicate that the fibre overgrowths associated with SMT deformation are composed of quartz, muscovite, phengite, chlorite, and lawsonite. The Si content of the phengite is between 3.49 and 3.51 per formula unit. We also found veins of coarse dark green jadeite crosscut by a semi-penetrative SMT cleavage.

In the Yolla Bolly study area in northern California, fibre overgrowths in the sandstones are made up of quartz, lawsonite, aragonite, phengitic white mica, muscovite, and chlorite. The Si content of the fibrous phengite ranges between 3.50 and 3.58 per formula unit (Ring 1996). Crosscutting veins contain pumpellyite, aragonite, calcite, albite, and quartz. Sodic amphibole is present as a matrix phase. In metabasalt, aegirine–omphacitic pyroxene is found as rims or replacement of original igneous clinopyroxene (Blake *et al.* 1988), and sodic amphibole is present as a matrix phase or replacing igneous hornblende.

The high Si content of the phengite (Massone & Schreyer 1987) and the presence of lawsonite,

aragonite, and jadeite in veins and fibres demonstrate that SMT deformation coincided with high-pressure metamorphism. Ductile strain may have continued to accumulate after peak metamorphism but for how much longer is not known.

Methods

Our study employs some new methods for measuring deformation in sandstones deformed by the SMT mechanism. Traditional methods, such as the R_f/ϕ method, are not suitable because the grains did not deform as passive markers but rather by modification of their external shapes. The projected dimension strain (PDS) and mode methods (Brandon *et al.* 1994; Feehan & Brandon 1999) were used to measure contractional and extensional strains, respectively. The SDA-fibre method was used to estimate internal rotation. These methods are briefly summarized here. (All of the programs developed and used in this study are available from the Web in both compiled and source-code forms at http://love.geology.yale.edu/~brandon/brandon.html. They are written in Microsoft Professional Basic 7.0 and will run on a DOS or Windows computer using any standard printer.)

The first step is to determine the principal directions for SMT strain. The principal stretches themselves are designated as $S_X \geq S_Y \geq S_Z$, where S is the final length/initial length. The cleavage plane is assumed to lie perpendicular to Z. To determine the X direction, we measured the average orientation of directed fibre overgrowths in a cleavage-parallel (XY) thin section. Y is then defined by its orthogonality with X and Z. With this information, we are able to cut an XZ thin section.

Most samples (36 of 64) have unidirectional fibres where both the XY and XZ sections showed well-organized fibre overgrowths oriented in the X direction (Fig. 2a, b and d). This textural relationship indicates that only one of the principal stretches is extensional. For these samples, the strain type is constrictional or plane with $S_X \geq 1 \geq S_Y \geq S_Z$. The remaining samples (28 of 64) have multidirectional fibres defined by coplanar fibres radiating out in all directions in the XY plane (Fig. 2c). This texture indicates a flattening-type strain with $S_X \geq S_Y > 1 \geq S_Z$.

The mode method

The mode method is used to determine the extensional strain recorded by the fibre overgrowths. The modal abundance of fibres was determined by line traverses using a computer-driven micron-stepping petrographic microscope. Modes were measured in the XZ section for unidirectional fibres and in the XY section for multidirectional fibres. In the first case, the maximum stretch S_X is related to the modal fraction of fibre m by the relationship $S_X = 1/(1-m)$. In the second case, extension has occurred in both the X and Y directions, so we can only determine the area dilatancy in the XY section, defined by the product $S_X S_Y$ = final area/initial area = $1/(1 - m)$. Other information, introduced below, must be used to determine directions and magnitudes for S_X and S_Y.

The more common and less time-consuming method for determining extension from fibre overgrowths involves measuring the length of the fibres relative to the section radius of the associated host grain (e.g. p. 271 in Ramsay & Huber 1983). We prefer our method because it provides a more direct measurement of the bulk extensional strain in the rock. Furthermore, our experience indicates that relative to the mode method, the fibre-length method commonly overestimates the extensional strain, perhaps because longer, better developed fibres are favoured when making length measurements.

A contractional principal direction, where $S \leq 1$, is characterized by an absence of fibre overgrowths parallel to that direction and by selvages and truncated grain boundaries lying perpendicular to that direction. Selvages can form in more than one orientation. Such a situation is expected where more than one principal direction is contractional. In this case, hand samples typically show a single well-developed cleavage, oriented perpendicular to Z, but observations with a petrographic microscope will reveal the presence of selvages in both the XY and XZ sections. Samples with $1 > S_Y \approx S_Z$ are characterized by the lack of a well-defined cleavage in hand sample. For these samples, thin section observations generally show many orientations of well-developed selvages, all of which are cozonal with X.

The PDS method

The PDS method is used to measure the amount of shortening produced by dissolution of grain boundaries. The method exploits the fact that for SMT deformation, the size of the detrital grains remains unchanged in length parallel to the X direction. The projected dimension of a grain is equivalent to its caliper dimension. The main idea behind the PDS method is that a contractional stretch in a specific direction in the rock must be accompanied by a reduction of the average caliper dimension of the grains in that direction by a factor equal to the stretch. In comparison, the average initial caliper dimension of a detrital grain is preserved in the X direction because the grains lack any significant internal deformation and because original grain boundaries are preserved in that direction beneath a mantle of fibre overgrowths. Therefore, a contractional principal stretch could be determined if we could measure the average caliper dimension of a large number of grains in a direction parallel to that principal direction and then divide that average by the average caliper dimension in the X direction.

A practical problem is that our measurements are made in two-dimensional thin sections, and yet the necessary caliper dimensions should be made in three dimensions. This problem can be accurately accounted for using a simple correction based on the relationship between section measurements and volume measurements for truncated spheres (see Feehan & Brandon (1998) for further details). The correction works well as long as the aspect ratio of the

initial grains is less than 3:1, which is commonly the case for sandstones (Paterson & Yu 1994; Ramthun *et al.* 1997). Our section measurements were made using a petrographic microscope with a drawing tube and digitizing tablet. Measurements are precise to better than ± 3 μm.

We have tested the PDS method using undeformed sandstone samples and found that it is relatively insensitive to primary grain fabrics that might be produced during deposition and compaction (Paterson & Yu 1994; Ramthun *et al.* 1997). Table 2 presents PDS measurements for seven samples of Great Valley sandstones unaffected by SMT deformation. For these samples, and others like them, we find that the average stretch is approximately one, as would be expected given the absence of SMT deformation. Deposition and compaction can produce a weak preferred orientation in grain shape. The PDS method, however, is based on the average projected dimension of the grains, and not on their orientations. Thus, the method is uniquely suited for measuring SMT strains in sandstones, but only as long as the assumption of no intragranular deformation holds (i.e. strains caused by dislocation glide are nil).

Next, we summarize uncertainties for our measurements. Orientation errors are estimated to be less than about ± 7°. To estimate uncertainties for the principal stretches, we accounted for the variance associated with the initial grain fabric as indicated by our PDS measurements from 'undeformed' sandstones (e.g. Table 2) and the variance associated with measurement errors as indicated by the bootstrap method of Efron (1982). These calculations indicate relative standard errors of *c.* 5%. In other words, a typical shortening stretch of 0.70 would have an absolute standard error of *c.* 0.035. The volume stretch, S_V, i.e. the final volume/initial volume, is defined by the product of the three principal stretches $S_V = S_X \cdot S_Y \cdot S_Z$. Propagation of standard errors for the principal stretches indicates that the relative standard error for S_V is *c.* 9%. Thus, a typical S_V = 0.66 would have an absolute standard error of *c.* 0.06.

The SDA-fibre method

The SDA-fibre method is used to measure the internal rotation associated with SMT deformation and the orientation and magnitude of S_X and S_Y for samples having multidirectional fibres in the XY section. This method was developed by Brandon and a full description has yet to be published. The following brief summary should be sufficient for our purposes here. The two published methods for analysis of syntectonic fibre overgrowths are the rigid-fibre method (Durney & Ramsay 1973; Ramsay & Huber 1983) and the deformable-fibre method (Ramsay & Huber 1983; Ellis 1986). In the first method, the fibres and grains are assumed to remain undeformed. The only motion that is allowed is that associated with separation and growth of new fibres at the grain–fibre interface. The growth of fibres on pyrite framboids is commonly approximated by this model (p. 265 in Ramsay & Huber 1983). The bulk deformation causes the fibres to be translated and rotated relative to the sites of fibre accretion. Thus, the shape of the fibres is formed as the fibre grows, and not by deformation of pre-existing fibres. The deformable-fibre model also has fibres growing parallel to the current incremental extension direction, but after initial growth, the fibres deform in the same manner as the bulk rock. For this case, it is necessary to incrementally undeform the fibre to recover the history of extensional stretching and rotation (Ramsay & Huber 1983; Ellis 1986).

Our textural observations indicate that neither of these models correctly represents the geometry of fibres growing on detrital grains in SMT-deformed sandstones. Fibre bundles that lie between two detrital grains commonly show a 'bow tie' geometry with the central segment of the fibre bundle being much thinner than its ends. These fibre bundles commonly show continuity along their entire length, indicating that new material was added at the inference between fibre bundles and their host grains. The mineralogical contrast between fibre and grain ensures that this interface is crystallographically incoherent. This type of fibre growth was called 'pyrite-type' or antitaxial growth by Ramsay & Huber (1983). We interpret the thinned central region of the fibre bundle to have formed by dissolution and shortening between adjacent fibres within the bundle. This conclusion is supported by the observation that the degree of thinning is commonly much more pronounced in the XZ section, where contractional strains are greater. Many

Table 2. *PDS ratios measured for undeformed Great Valley sandstones*

	PDS ratios		
Sample	AB	AC	BC
GV 93-1	0.958	1.101	1.096
GV 93-2	1.034	1.057	1.147
GV 93-5	0.996	1.197	1.333
GV 93-6	1.113	0.991	1.060
GV 93-45	1.012	0.993	1.078
GV 93-52	0.978	1.011	0.989
GV 93-55	1.067	0.981	0.998
Log mean	1.02	1.04	1.09

AB, AC, and BC define three orthogonal thin sections, with AB parallel to bedding.

of the *XY* sections, which typically have S_Y close to unity, show relatively straight fibre bundles, with little to no thinning. These examples are similar to those shown by Ramsay & Huber (1983) to support their model of rigid-fibre overgrowths on pyrite grains.

We conclude that the SMT fibres in our sandstones do not fit the rigid-fibre model unless the contractional principal stretches are close to one. We also reject the deformable-fibre model because the fibres show no evidence that they were stretched or broken along their length. Extension appears to have been accommodated entirely by separation and growth of new fibre at the grain–fibre interface. In our view, the fibres were deformed only by dissolution and progressive thinning, which is most pronounced in the oldest parts of the fibre, located in the central segment. The deformable-fibre model specifies that, once formed, the fibres behaved as passive markers. At higher temperatures, this description might hold, but the temperatures associated with SMT deformation in our samples were too low for fibres to deform internally by intracrystalline mechanisms.

Brandon has developed two computer programs, similar in some respects to the one described by Ellis (1986), that analyse the growth of semi-deformable antitaxial fibres. The basic idea is that fibres are allowed to grow only at the grain–fibre interface, and once formed, they are allowed to shorten only perpendicular to the current incremental shortening direction. One of the programs (FBR-SIM) simulates the progressive growth of the fibres on a section through the centre of an 'average' three-dimensional detrital grain. The finite deformation is determined by integrating a constant velocity–gradient tensor. The evolving geometry of the fibres and the progressive orientation of the cleavage selvages are determined by calculating the displacement paths for particle points that originated at the grain boundary or within the cleavage selvage. The simulation can account for a general three-dimensional deformation including internal rotation. Some examples of simulated fibre overgrowths are shown in Fig. 3. We have found that the simulation program closely reproduces the size and form of unidirectional and multidirectional fibres in sections with different strains and degrees of internal rotation.

To analyse fibre overgrowths in our samples, Brandon designed a second program (FIBER), which includes the simulation routine and an inverse algorithm. The objective is to find the forward model that best represents the fibre trajectories in each thin section. A best-fit solution is found by using a non-linear least-squares algorithm based on the simplex method (Amoeba routine of Press *et al.* (1992, p. 402)). The required input data for each section includes the modal abundance of fibre, the average orientation of the selvages, and the digitized shapes of a random sample of about 30–40 non-truncated fibres. For sections with unidirectional fibres, the input must also include the contractional principal stretch for that section, as determined by the PDS method. The program calculates the best-fit solution for the internal rotation in that section. For sections with multidirectional fibres, it also gives the best estimate of the directions and magnitudes of the two extensional principal stretches. It should be noted that the program does not depend on the diameter of the host grains, but instead uses the mode and shape of the fibres to estimate the average section radius of the host grains.

To estimate the internal rotation in three dimensions, the components of the internal rotation vector are measured in the *XY* and *XZ* sections. (There is generally no record of internal rotation in the *YZ* section because fibres are typically small or absent in that section.) Each measured component is cast as a vector oriented normal to its section with a magnitude equal to the measured rotation angle. These components are then summed to give the internal rotation vector. The result is reported in Table 3 as a rotation axis and a finite rotation angle Ω_i with a positive angle indicating a right-handed rotation. Vector addition of finite rotations is appropriate as long as the rotation angles are less than *c.* 5° (p. 236 in Cox & Harte (1986)). Above this limit, the magnitude of the summed rotation remains fairly precise but the orientation of the rotation axis becomes increasingly imprecise. It should be noted that the FIBER program failed to find a stable solution for internal rotations for 15 samples (dashed entries in Tables 3 and 4). This problem typically occurs when fibres are very short or too variable in orientation.

More could be said about our SDA-fibre method, but for this study, the method provides quantitative support for a conclusion that is fairly obvious from the textures themselves. Namely, SMT deformation in the Eastern Belt involved only minor internal rotation and was approximately coaxial. The main evidence is that in *XZ* sections, the fibre overgrowths, which record the progressive orientation of the incremental extension direction, are, on average, parallel to the trace of cleavage (Fig. 2d), which marks the approximate orientation of the finite extension direction. This concordance indicates that there was little significant rotation of the incremental extension direction relative to the evolving finite extension direction. As a contrary example, the simulated simple-shear fabric illustrated in Fig. 3b shows a discordance of 21° between the orientation of fibres and the trace of cleavage in the *XZ* section (Fig. 3). Strongly asymmetric fabrics like this are not observed in our samples.

The finite strain and internal rotation data were used to calculate average kinematic numbers (p. 16 in Passchier & Trouw (1996)). Means *et al.* (1980) proposed using the kinematic vorticity number W_k as a measure of the non-coaxiality of the deformation, where

$$W_k = \frac{w}{\sqrt{2}\, D_T}$$

In this equation, w is the magnitude of the internal vorticity vector, given by $w = 2\left[w_{32}^2 + w_{13}^2 + w_{21}^2\right]^{1/2}$, where w_{ij} are the components of the internal vorticity tensor (equation (18) of Means *et al.* (1980)). D_T is a scalar measure of the average strain rate given by $D_T = \left[D_1^2 + D_2^2 + D_3^2\right]^{1/2}$, where D_1, D_2, and D_3 are the principal values of the stretching tensor D_{ij} (see pp. 145–150 in Malvern (1969), for more details about w_{ij}

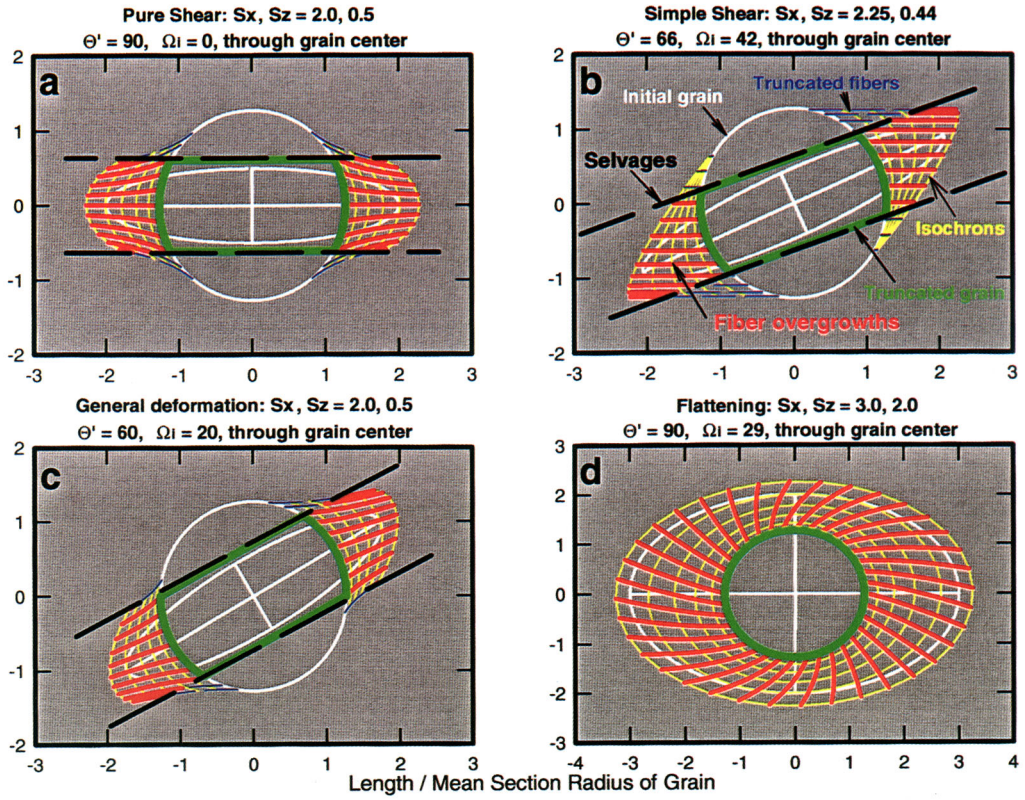

Fig. 3. Examples of SMT fabrics predicted by the semi-deformable antitaxial (SDA) fibre model. The figures are representative of the 'average' geometry of the deformation fabric through the centre of an average grain in the XZ section. Dimensions are normalized to the mean section radius of the deforming grain. (Note that the true radius of a spherical grain, which is the outline shown in the diagrams, is 1.27 times the mean radius of all sections through the sphere.) S_X and S_Z are the principal stretches in the X and Z directions. The angle Θ' refers to the clockwise angle of X relative to the vertical axis. The internal rotation axis is parallel to Y and the internal rotation angle is reported as Ω_i. An interesting result is that coaxial deformation can produce curved fibres (**a**) and non-coaxial deformation can produce straight fibres (**b**). The degree of non-coaxiality is best judged by the average angle between cleavage and the fibre overgrowths.

and D_{ij}). Passchier (1991) defined the kinematic dilatancy number A_k as a relative measure of the volume strain rate with respect to the average strain rate. Generalizing his definition to three dimensions gives

$$A_k = \frac{D_V}{\sqrt{2}\, D_T}$$

where $D_V = D_1 + D_2 + D_3$ is the volume strain rate. When considering a general deformation that might included a volume strain, it is advantageous to replace D_T with a scalar measure of the deviatoric strain rate defined by

$$D_D = \left[(1/3)\left((D_1 - D_2)^2 + (D_2 - D_3)^2 + (D_1 - D_3)^2\right)\right]^{1/2}$$

(compare equation (6) in Brandon (1995)). D_D describes the average rate of distortion caused by the deformation; it is proportional to the average shear strain rate and independent of the volume strain rate. It should be noted that $D_T^2 = D_D^2 + D_V^2$. The modified kinematic numbers, distinguished by asterisks, are

$$W_k^* = \frac{w}{\sqrt{2}\, D_D} \quad \text{and} \quad A_k^* = \frac{D_V}{\sqrt{2}\, D_D}$$

A coaxial deformation has $W_k = W^*_k = 0$ and a simple-shear deformation with no volume strain has $W_k = W^*_k = 1$. However, it should be noted that for simple shear with a volume strain, W^*_k remains equal to one, but W_k is no longer one and can take on any value. This example illustrates why we prefer the modified kinematic numbers. $A^*_k = 0$ indicates that the deformation is isochoric, $A^*_k > 0$ indicates a dilatant deformation, and $A^*_k < 0$ a compactive deformation. For example, a deformation involving uniaxial shortening and an

Table 3. *Measurements of SMT deformation relative to present coordinates*

	Principal stretches															
	Extension			Intermediate			Shortening			Volume	Internal rotation			Kinematic numbers		
No.	tr.	pl.	S_X	tr.	pl.	S_Y	tr.	pl.	S_Z	S_V	tr.	pl.	Ω_i	W_m	W^*_m	A^*_m
Valentine Springs Formation, Yolla Bolly Mountains																
1	5	14	1.49	102	27	0.82	251	59	0.47	0.57	103	31	+7.0	0.21	0.23	–0.48
2	348	26	1.35	104	42	0.70	239	38	0.58	0.55	255	9	+8.5	0.31	0.36	–0.68
3	69	13	1.17	174	49	0.94	328	38	0.33	0.36	326	42	+2.4	0.05	0.06	–0.75
4	202	17	1.13	80	60	1.06	300	24	0.60	0.72	–	–	–	–	–	–0.47
Yolla Bolly terrane, Yolla Bolly Mountains																
5	89	33	1.33	202	31	0.76	323	41	0.66	0.67	279	56	–9.8	0.43	0.47	–0.54
6	42	8	1.08	139	42	1.06	303	47	0.53	0.61	–	–	–	–	–	–0.62
7	241	25	1.52	148	7	0.70	44	64	0.69	0.73	93	61	–5.6	0.21	0.22	–0.34
8	65	3	1.34	156	20	0.81	327	70	0.74	0.80	159	56	+3.7	0.19	0.20	–0.34
9	63	1	1.21	153	12	1.10	326	78	0.59	0.79	167	84	–9.0	0.39	0.40	–0.31
10	104	1	1.06	194	26	1.05	11	64	0.58	0.65	–	–	–	–	–	–0.63
11	295	28	1.22	174	44	1.21	45	33	0.56	0.83	57	45	–6.3	0.24	0.25	–0.21
12	153	54	1.14	54	6	0.75	320	35	0.74	0.63	54	6	+0.0	0.00	0.00	–0.93
13	49	2	1.09	143	63	1.06	317	27	0.54	0.62	139	26	–1.1	0.04	0.05	–0.59
14	297	17	1.47	64	63	0.84	200	20	0.64	0.79	174	60	–1.2	0.05	0.05	–0.28
15	133	6	1.08	228	40	1.01	35	50	0.54	0.59	–	–	–	–	–	–0.69
16	357	24	1.09	266	2	0.78	172	65	0.77	0.65	–	–	–	–	–	–1.08
17	69	19	1.40	330	26	0.75	192	57	0.69	0.72	176	38	+3.4	0.15	0.15	–0.42
18	348	34	1.26	255	4	1.15	159	55	0.66	0.96	126	47	–11.3	0.56	0.56	–0.06
19	356	15	1.30	255	36	1.06	104	50	0.69	0.95	226	68	–5.3	0.29	0.29	–0.08
20	45	10	1.20	314	8	1.19	188	76	0.60	0.86	167	69	+4.0	0.17	0.18	–0.19
Yolla Bolly terrane, Leech Lake Mountain																
21	83	8	1.14	345	45	1.09	181	44	0.61	0.76	184	53	+4.9	0.23	0.25	–0.40
22	284	2	1.36	14	4	0.75	167	85	0.72	0.73	190	59	+8.9	0.43	0.46	–0.43
23	270	6	1.14	3	23	1.08	167	66	0.67	0.82	158	75	+2.4	0.14	0.14	–0.33
24	101	26	1.07	350	37	1.06	217	42	0.64	0.73	212	36	–1.6	0.09	0.09	–0.54
25	137	2	1.10	45	30	1.08	230	60	0.61	0.72	258	86	+1.3	0.06	0.07	–0.48
26	91	19	1.32	183	6	1.06	290	70	0.61	0.85	336	50	–8.0	0.35	0.35	–0.20
27	284	3	1.17	193	25	0.66	20	65	0.63	0.49	19	61	–18.4	0.72	0.94	–1.03
28	329	11	1.36	92	71	0.67	236	15	0.61	0.56	61	10	–7.0	0.24	0.28	–0.67
29	106	13	1.33	5	37	0.70	212	50	0.54	0.50	294	76	+6.7	0.23	0.27	–0.74
30	15	22	1.10	109	11	1.01	225	65	0.65	0.72	139	55	+0.9	0.05	0.06	–0.58
31	59	8	1.10	325	27	0.83	164	62	0.64	0.58	168	67	+1.1	0.06	0.07	–0.99
32	6	24	1.20	98	6	1.00	202	65	0.53	0.64	108	26	–1.1	0.04	0.04	–0.53

Table 3. *continued*

	Principal stretches															
	Extension			Intermediate			Shortening			Volume	Internal rotation			Kinematic numbers		
No.	tr.	pl.	S_X	tr.	pl.	S_Y	tr.	pl.	S_Z	S_V	tr.	pl.	Ω_i	W_m	W^*_m	A^*_m
33	319	21	1.03	64	35	1.03	204	48	0.55	0.58	119	68	–0.1	0.00	0.00	–0.74
34	312	10	1.13	51	43	1.07	212	45	0.50	0.60	211	49	–1.5	0.05	0.06	–0.55
35	296	11	1.31	38	47	0.66	196	41	0.62	0.54	202	24	+5.8	0.21	0.24	–0.75
36	225	2	1.01	134	26	1.00	320	64	0.54	0.55	316	19	+0.0	0.00	0.00	–0.85
37	328	43	1.00	110	41	0.72	218	20	0.63	0.45	70	13	+0.0	0.00	0.00	–1.66
38	3	43	1.12	131	34	1.11	243	29	0.62	0.77	263	10	–0.2	0.01	0.01	–0.38
39	337	12	1.00	98	67	0.87	243	19	0.81	0.70	223	62	+0.0	0.00	0.00	–1.63
40	287	22	1.28	28	25	0.82	161	56	0.58	0.61	42	46	+3.5	0.14	0.15	–0.63
Yolla Bolly terrane, Mount Hamilton, Diablo Range																
41	21	54	1.27	142	20	0.71	243	28	0.54	0.49	221	34	+3.3	0.11	0.13	–0.82
42	33	14	1.06	300	14	1.06	168	70	0.49	0.55	167	70	+0.5	0.02	0.02	–0.67
43	168	50	1.06	318	36	0.78	59	15	0.50	0.41	–	–	–	–	–	–1.17
44	323	46	1.04	202	26	1.04	94	32	0.63	0.68	–	–	–	–	–	–0.66
45	315	34	1.22	201	31	0.77	80	40	0.64	0.60	47	3	–0.8	0.04	0.04	–0.77
46	111	54	1.19	249	28	0.66	350	20	0.62	0.49	234	21	+2.8	0.11	0.14	–1.00
47	317	36	1.04	213	19	1.04	100	48	0.62	0.67	206	27	–0.9	0.05	0.05	–0.67
48	7	61	1.09	253	13	0.84	157	25	0.56	0.51	–	–	–	–	–	–1.00
49	158	35	1.02	56	17	0.79	304	50	0.50	0.40	–	–	–	–	–	–1.26
50	219	61	1.10	1	24	1.09	98	16	0.70	0.84	–	–	–	–	–	–0.34
51	187	19	1.22	74	49	0.83	291	35	0.60	0.61	8	71	–2.7	0.12	0.13	–0.70
52	232	60	1.30	119	12	0.76	23	27	0.59	0.58	130	6	+7.1	0.29	0.33	–0.67
53	232	30	1.06	140	4	0.96	43	60	0.66	0.67	–	–	–	–	–	–0.80
54	192	17	1.07	101	4	0.75	357	72	0.46	0.37	–	–	–	–	–	–1.18
55	233	27	1.01	134	17	1.01	15	57	0.45	0.46	–	–	–	–	–	–0.83
56	235	26	1.05	61	64	1.04	325	3	0.61	0.67	33	63	–4.7	0.23	0.26	–0.65
Yolla Bolly terrane, Pacheco Pass, Diablo Range																
57	24	5	1.14	292	17	1.03	130	72	0.66	0.77	128	70	+1.7	0.10	0.10	–0.44
58	36	24	1.02	164	54	0.66	294	25	0.50	0.34	–	–	–	–	–	–1.52
59	248	35	1.04	148	14	1.01	40	51	0.57	0.60	–	–	–	–	–	–0.76
60	245	2	1.25	155	7	1.05	355	83	0.51	0.67	342	72	+4.6	0.16	0.17	–0.42
61	18	15	1.15	270	51	0.60	119	35	0.49	0.34	119	35	+9.1	0.27	0.38	–1.22
62	103	32	1.17	10	5	0.89	272	58	0.62	0.65	271	58	+1.9	0.09	0.10	–0.69
63	280	8	1.14	184	35	0.97	21	54	0.53	0.59	21	54	–4.0	0.15	0.17	–0.66
64	191	7	1.21	98	23	0.69	297	66	0.66	0.55	–	–	–	–	–	–0.88

tr. and pl. indicate trend and plunge. A right-handed internal rotation is indicated by a positive angle.

Table 4. *Measurements of SMT deformation after unfolding of the effects of late-stage shallow folding*

	Principal stretches														
	Extension			Intermediate			Shortening			Volume	Internal rotation			Kinematic numbers		
No.	tr.	pl.	S_X	tr.	pl.	S_Y	tr.	pl.	S_Z	S_V	tr.	pl.	Ω_i	W_m	W^*_m	A^*_m
Valentine Springs Formation, Yolla Bolly Mountains																
1	196	13	1.49	101	18	0.82	319	67	0.47	0.57	100	22	+7.0	0.21	0.23	–0.48
2	7	4	1.35	100	32	0.70	273	58	0.58	0.55	277	25	+8.5	0.31	0.36	–0.68
3	69	13	1.17	175	49	0.94	328	38	0.33	0.36	327	42	+2.4	0.05	0.06	–0.75
4	202	17	1.13	80	60	1.06	300	24	0.60	0.72	–	–	–	–	–	–0.47
Yolla Bolly terrane, Yolla Bolly Mountains																
5	100	46	1.33	192	3	0.76	286	43	0.66	0.67	243	37	–9.8	0.43	0.48	–0.54
6	42	8	1.08	139	41	1.06	303	47	0.53	0.61	–	–	–	–	–	–0.62
7	241	25	1.52	148	6	0.70	44	64	0.69	0.73	94	61	–5.6	0.21	0.22	–0.34
8	65	3	1.34	156	20	0.81	327	70	0.74	0.80	159	56	+3.7	0.19	0.20	–0.34
9	63	1	1.21	153	12	1.10	326	78	0.59	0.79	167	84	–9.0	0.39	0.40	–0.31
10	104	1	1.06	195	26	1.05	11	64	0.58	0.65	–	–	–	–	–	–0.63
11	295	28	1.22	177	44	1.21	45	33	0.56	0.83	58	46	–6.2	0.24	0.24	–0.21
12	161	48	1.14	54	15	0.75	311	39	0.74	0.63	54	15	+0.0	0.00	0.00	–0.93
13	48	11	1.09	156	58	1.06	310	29	0.54	0.62	142	23	–1.1	0.04	0.05	–0.59
14	302	17	1.47	57	55	0.84	203	29	0.64	0.79	166	68	–1.2	0.05	0.05	–0.28
15	134	8	1.08	233	49	1.01	36	40	0.54	0.59	–	–	–	–	–	–0.69
16	185	2	1.09	276	17	0.78	92	73	0.77	0.65	–	–	–	–	–	–1.08
17	252	4	1.40	342	9	0.75	140	81	0.69	0.72	156	59	+3.4	0.15	0.15	–0.42
18	0	10	1.26	266	23	1.15	113	64	0.66	0.96	101	43	–11.3	0.56	0.56	–0.06
19	352	23	1.30	249	29	1.06	114	52	0.69	0.95	220	59	–5.3	0.29	0.29	–0.08
20	231	18	1.20	141	1	1.19	47	72	0.60	0.86	21	69	+4.0	0.17	0.18	–0.19
Yolla Bolly terrane, Leech Lake Mountain																
21	273	7	1.14	6	26	1.09	166	67	0.61	0.76	155	76	+5.0	0.24	0.25	–0.40
22	297	7	1.36	204	24	0.75	43	66	0.72	0.73	140	82	+9.0	0.44	0.46	–0.43
23	286	17	1.14	195	3	1.08	95	73	0.67	0.82	67	69	+2.0	0.12	0.12	–0.33
24	101	17	1.07	7	13	1.06	241	69	0.64	0.73	229	64	–2.0	0.11	0.12	–0.54
25	144	12	1.10	53	3	1.08	308	78	0.61	0.72	28	64	+1.0	0.05	0.05	–0.48
26	96	6	1.32	190	32	1.06	356	57	0.61	0.85	2	28	–8.0	0.35	0.35	–0.20
27	297	8	1.17	198	52	0.66	33	37	0.63	0.49	32	33	–18.0	0.70	0.92	–1.03
28	161	5	1.36	64	51	0.67	255	38	0.61	0.56	252	13	–7.0	0.24	0.28	–0.67
29	111	7	1.33	19	10	0.70	237	78	0.54	0.50	7	59	+7.0	0.24	0.28	–0.74
30	206	6	1.10	115	7	1.01	333	81	0.65	0.72	106	56	+1.0	0.06	0.06	–0.58
31	251	15	1.10	344	11	0.83	107	71	0.64	0.58	91	74	+1.0	0.05	0.06	–0.99

Table 4. *continued*

	Principal stretches														
	Extension			Intermediate			Shortening			Volume	Internal rotation			Kinematic numbers		
No.	tr.	pl.	S_X	tr.	pl.	S_Y	tr.	pl.	S_Z	S_V	tr.	pl.	Ω_i	W_m	W^*_m	A^*_m
32	198	3	1.20	288	3	1.00	55	87	0.53	0.64	107	20	–1.0	0.04	0.04	–0.53
33	336	8	1.03	67	12	1.03	213	76	0.55	0.58	77	56	+0.0	0.00	0.00	–0.74
34	325	1	1.13	55	17	1.07	233	73	0.50	0.60	233	10	–2.0	0.07	0.08	–0.55
35	312	9	1.31	45	19	0.66	197	69	0.62	0.54	211	52	+6.0	0.22	0.25	–0.75
36	238	28	1.01	129	32	1.00	4	47	0.54	0.55	333	7	+0.0	0.00	0.00	–0.85
37	353	24	1.00	99	33	0.73	234	47	0.63	0.45	259	7	+0.0	0.00	0.00	–1.66
38	19	16	1.12	121	37	1.11	270	49	0.62	0.77	281	25	+0.0	0.00	0.00	–0.38
39	168	7	1.00	70	49	0.87	265	40	0.81	0.70	314	81	+0.0	0.00	0.00	–1.63
40	309	23	1.28	218	3	0.82	120	67	0.58	0.61	48	19	+4.0	0.16	0.18	–0.63
Yolla Bolly terrane, Mount Hamilton, Diablo Range																
41	23	29	1.27	122	17	0.71	237	56	0.54	0.49	202	61	+3.3	0.11	0.13	–0.82
42	33	14	1.06	300	14	1.06	168	70	0.49	0.55	167	70	+0.5	0.02	0.02	–0.67
43	202	23	1.06	307	31	0.78	82	50	0.50	0.41	–	–	–	–	–	–1.17
44	301	40	1.04	38	9	1.04	138	48	0.63	0.68	–	–	–	–	–	–0.66
45	306	28	1.22	38	3	0.77	136	62	0.64	0.60	196	33	–0.8	0.04	0.04	–0.77
46	111	54	1.19	249	28	0.66	350	20	0.62	0.49	234	21	+2.8	0.11	0.14	–1.00
47	306	30	1.04	47	18	1.04	163	54	0.62	0.67	53	26	–0.9	0.05	0.05	–0.67
48	17	30	1.09	246	48	0.84	124	25	0.56	0.51	–	–	–	–	–	–1.00
49	117	33	1.02	221	20	0.79	337	50	0.50	0.40	–	–	–	–	–	–1.26
50	232	33	1.10	357	42	1.09	119	31	0.70	0.84	–	–	–	–	–	–0.34
51	154	39	1.22	54	13	0.83	310	49	0.60	0.61	25	39	–2.7	0.12	0.13	–0.70
52	242	22	1.30	144	19	0.76	19	60	0.59	0.58	149	7	+7.1	0.29	0.33	–0.67
53	65	7	1.06	335	1	0.96	237	83	0.66	0.67	–	–	–	–	–	–0.80
54	192	17	1.07	101	5	0.75	357	72	0.46	0.37	–	–	–	–	–	–1.18
55	66	10	1.01	158	13	1.01	300	73	0.45	0.46	–	–	–	–	–	–0.83
56	254	50	1.05	28	30	1.04	132	22	0.61	0.67	42	35	–4.7	0.23	0.26	–0.65
Yolla Bolly terrane, Pacheco Pass, Diablo Range																
57	24	5	1.14	293	18	1.03	130	72	0.66	0.77	127	69	+1.7	0.10	0.10	–0.44
58	207	3	1.02	113	53	0.66	299	36	0.50	0.34	–	–	–	–	–	–1.52
59	247	62	1.04	130	14	1.01	34	24	0.57	0.60	–	–	–	–	–	–0.76
60	245	2	1.25	155	6	1.05	355	84	0.51	0.67	342	73	+4.6	0.16	0.17	–0.42
61	21	39	1.15	266	28	0.60	151	38	0.49	0.34	151	38	+9.0	0.27	0.38	–1.22
62	85	11	1.17	178	15	0.89	319	71	0.62	0.65	320	71	+1.9	0.09	0.10	–0.69
63	111	8	1.14	202	12	0.97	347	75	0.53	0.59	346	75	–4.0	0.15	0.17	-0.66
64	191	7	1.21	98	23	0.69	297	66	0.66	0.55	–	–	–	—	—	-0.88

tr. and pl. indicate trend and plunge. A right-handed internal rotation is indicated by a positive angle.

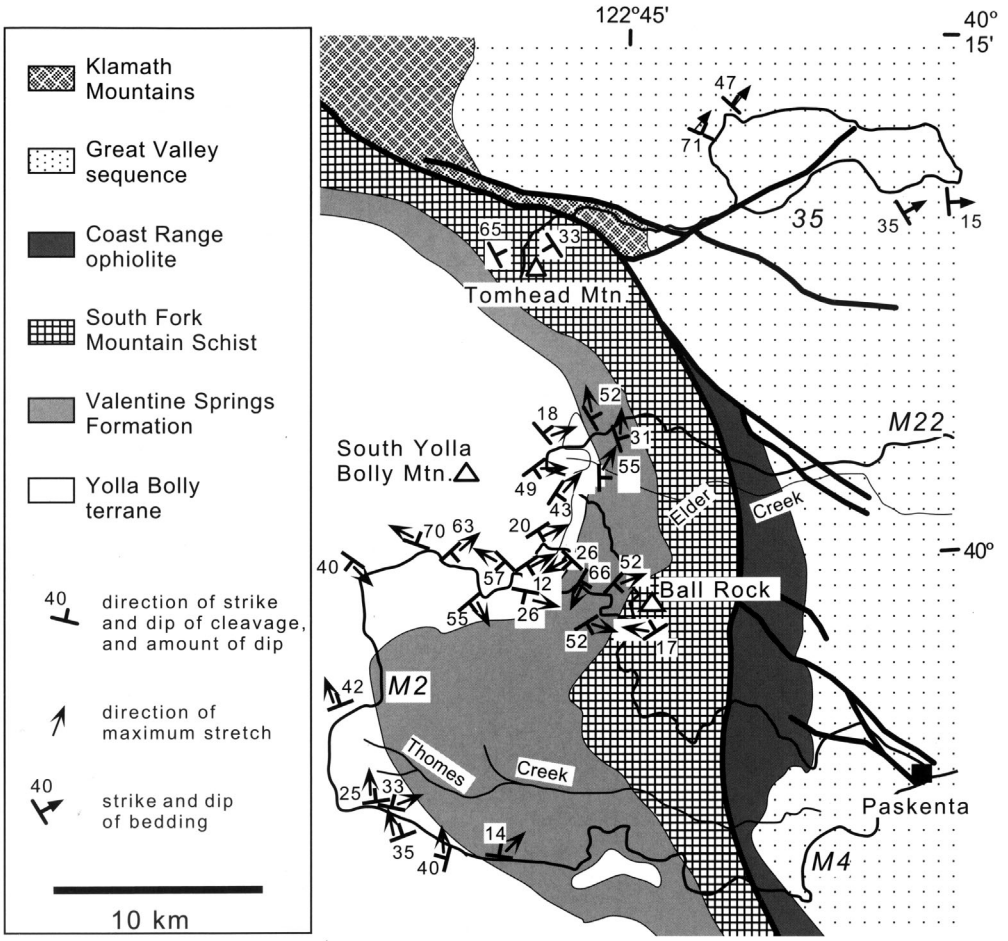

Fig. 4. Geological map of the Yolla Bolly Mountains study area showing principal stretch directions for SMT deformation in the Eastern Belt of the Franciscan Complex, which in this area includes the South Fork Mountain Schist, Valentine Springs Formation, and the Pickett Peak terrane. All directions are relative to present coordinates. Note the large degree of local variation in the principal directions. M2, M22, M4 and 35 refer to US Forest Service roads.

equal loss of volume, such as compaction in a sedimentary basin, would have $A^*_k = -1$ because the rates of volume strain and deviatoric strain would be equal in magnitude but opposite in sign.

The kinematic numbers are defined with respect to rates of deformation because they represent properties of the deformation at a point. They are, however, dimensionless, and therefore independent of the actual deformation rate. Application of these concepts to a finite deformation is complicated because the kinematic numbers associated with deformation at a material point can vary with time. None the less, one can define an average kinematic number by assuming a steady deformation and then finding an average set of rate parameters that when integrated give the observed finite deformation (Passchier 1988; Means 1994). (Note that as used here, steady means that the kinematic numbers at a material point remained constant with time, but it does not require that the rate of deformation remained constant.) The rate parameters are specified by the velocity gradient tensor ($\boldsymbol{L}$ of Malvern (1969)). The kinematic numbers can be directly calculated from the average $\boldsymbol{L}$. These average values are designated as W_m, W^*_m and A^*_m. The values reported in Tables 3 and 4 were calculated numerically by searching for the unique average $\boldsymbol{L}$ that when integrated gave the measured three-dimensional finite strain and internal rotation (see Feehan & Brandon (1999) for details about the numerical integration). The simple geometries associated with our fibre

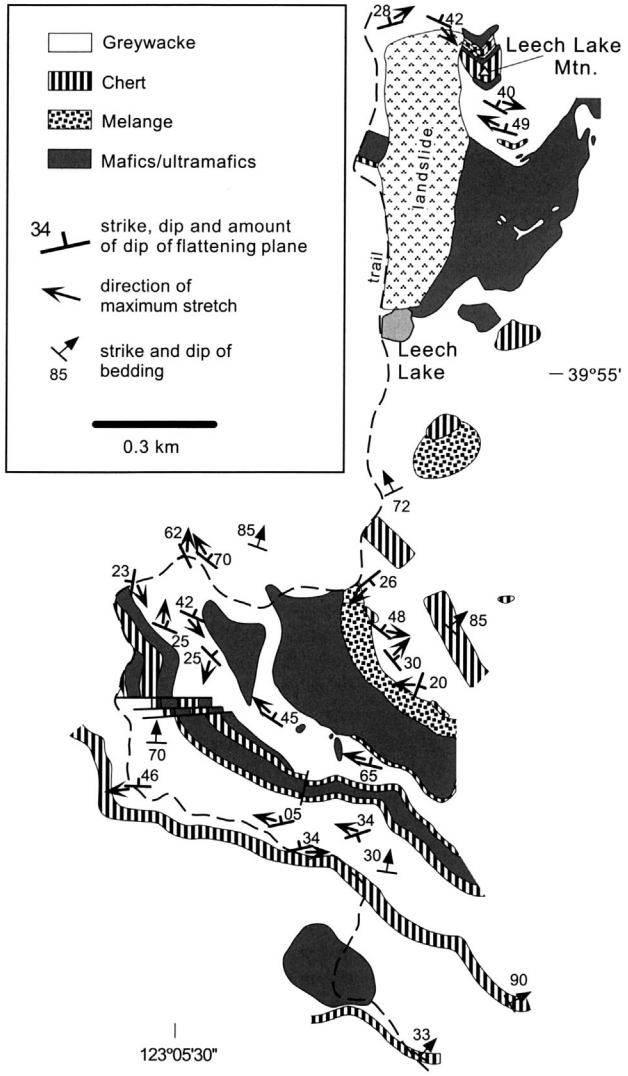

Fig. 5. Geological map of the Leech Lake Mountain study area showing principal stretch directions for SMT deformation. All directions are relative to present coordinates. Variability of principal directions is slightly less than that in the Yolla Bolly Mountains study area.

overgrowths indicate that SMT deformation in the Franciscan Complex probably did not depart strongly from the steady-deformation assumption used here.

Results

Sampling

To obtain reliable tensor averages for SMT deformation at a regional scale, we sampled randomly in regions where the rock types were homogeneous at the scale of sampling. We focused on two areas in northern California, located in the Yolla Bolly Mountains and at Leech Lake Mountain, and one in the Diablo Range of central California (Fig. 1a). All areas contain typical outcrops of the Eastern Belt. In the Yolla Bolly Mountains, we collected samples of metasandstones, metabasalt, shale and schist from the Pickett Peak terrane: one from the South Fork Mountain Schist and eight from the Valentine Springs Formation. Sixteen sandstone samples were collected from the Yolla Bolly terrane. Strain directions were

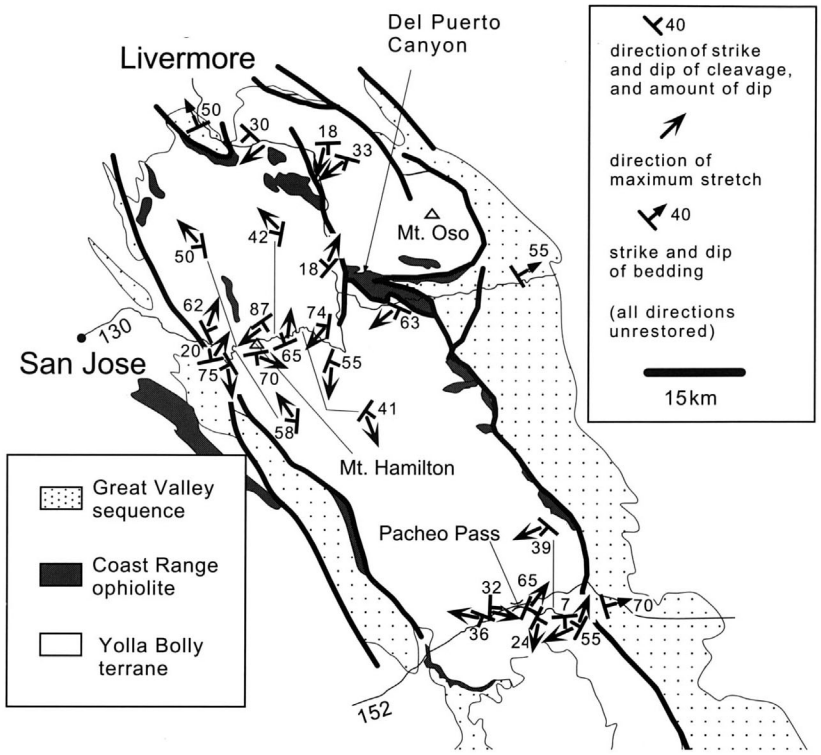

Fig. 6. Geological map of the Diablo Range with principal strain directions for SMT deformation. Mount Hamilton lies to the north and Pacheco Pass to the south. The variability in principal directions is similar to that in the Yolla Bolly Mountains. California State highways 130 and 152 are also shown.

determined for all and are shown in Fig. 4. Full deformation measurements were made for four of the Valentine Springs sandstones and all of the Yolly Bolly terrane samples. At Leech Lake Mountain (Fig. 5), we analysed 20 sandstones from the Yolla Bolly terrane. In the Diablo Range (Fig. 6), 16 sandstones for the Mt Hamilton–Mt Oso area and another eight sandstones from the Pacheco Pass area were analysed. Detailed descriptions of the geology of these study areas have been provided by Chesterman (1963), Worrall (1979, 1981), Blake *et al.* (1988), and Bolhar (1997) for the Yolla Bolly Mountains and Leech Lake Mountain, and Ernst (1965, 1987, 1993) and Cowan (1974) for the Diablo Range. Field measurements of cleavage, bedding, and stretching lineations were made for comparison with the deformation analysis.

Analysis

Our primary results are reported in Tables 3–5 and Fig. 7. The data are characterized in Fig. 8 according to strain symmetry (oblate v. prolate), strain type (constrictional v. flattening), and mean kinematic numbers.

An important initial observation is that individual principal strain directions and internal rotation axes are variable in orientation (e.g. Fig. 7). The observed variability is too large to be attributed to measurement error alone. Other studies (e.g. Feehan & Brandon 1999) suggest that SMT deformation might be typified by local-scale variability, especially in the orientation of X and Y. Thus, we have found it useful to calculate averages for these data (Table 5). As discussed by Brandon (1995), it is not appropriate to average the principal stretches, principal directions, and internal rotation measurements separately. The data must be averaged in tensor form to ensure that the orthogonality of the axes is preserved and that the magnitudes and directions of the principal stretches are correctly associated. If the rotational component of the deformation is fairly small, then one can average the stretch tensor and the internal rotation tensor separately, without introducing significant errors (Brandon 1995). Average stretches and internal rotations in Table 5 were

Table 5. *Regional averages for SMT deformation in present (P) and unfolded (U) coordinates*

	Principal stretches															
	Extension			Intermediate			Shortening			Volume	Internal rotation			Kinematic numbers		
P/U	tr.	pl.	S_X	tr.	pl.	S_Y	tr.	pl.	S_Z	S_V	tr.	pl.	Ω_i	W_m	W^*_m	A^*_m
Valentine Springs Formation, Yolla Bolly Mountains study area (N = 4)																
P	26	12	1.04	126	40	0.86	282	48	0.60	0.54	236	60	+2.7	0.11	0.16	-0.60
U	205	11	1.16	106	40	0.86	307	48	0.53	0.54	300	72	+2.8	0.10	0.11	–0.42
Yolla Bolly terrane, Yolla Bolly Mountains study area (N = 16)																
P	255	2	1.02	164	14	0.92	354	76	0.77	0.73	80	80	–2.7	0.25	0.30	–0.54
U	240	13	1.02	146	15	0.96	10	70	0.75	0.73	139	76	–2.4	0.22	0.26	–0.48
Yolla Bolly terrane, Leech Lake Mountain study area (N = 20)																
P	298	1	1.06	28	31	0.91	206	59	0.66	0.64	199	6	+1.4	0.08	0.09	–1.04
U	128	0	1.06	38	3	0.91	224	87	0.66	0.64	165	43	+1.0	0.05	0.06	–1.04
Grand mean for Yolla Bolly terrane, Yolla Bolly and Leech Lake Mountain study areas (N = 36)																
P	105	3	1.02	14	17	0.90	206	72	0.73	0.68	28	45	–1.3	0.09	0.12	–1.47
U	118	2	1.01	208	6	0.94	12	84	0.71	0.68	4	59	–0.5	0.04	0.04	–1.31
Yolla Bolly terrane, Mount Hamilton, Diablo Range study area (N = 17)																
P	196	23	0.90	303	34	0.82	80	47	0.76	0.56	356	7	–1.3	0.10	0.37	–1.58
U	37	0	0.95	307	10	0.84	130	80	0.70	0.56	189	6	+1.6	0.11	0.21	–0.85
Yolla Bolly terrane, Pacheco Pass, Diablo Range study area (N = 7)																
P	202	6	0.97	111	9	0.82	326	79	0.64	0.51	135	52	+2.6	0.13	0.19	–1.42
U	212	2	0.94	121	10	0.84	315	79	0.65	0.51	152	52	+2.6	0.13	0.17	–1.52
Grand mean for Yolla Bolly terrane, Diablo Range study area (N = 24)																
P	196	14	0.91	288	9	0.81	50	74	0.74	0.55	161	22	+1.4	0.10	0.28	–2.83
U	216	0	0.95	306	2	0.83	119	88	0.69	0.55	178	26	+1.7	0.11	0.18	–1.88
Grand mean, all study areas (N = 64)																
P	103	5	0.92	13	5	0.90	236	83	0.75	0.62	16	18	–1.0	0.08	0.12	–2.14
U	221	3	0.96	129	5	0.92	345	84	0.70	0.62	184	6	+0.6	0.04	0.05	–1.45

tr. and pl. indicate trend and plunge. A right-handed internal rotation is indicated by a positive angle.

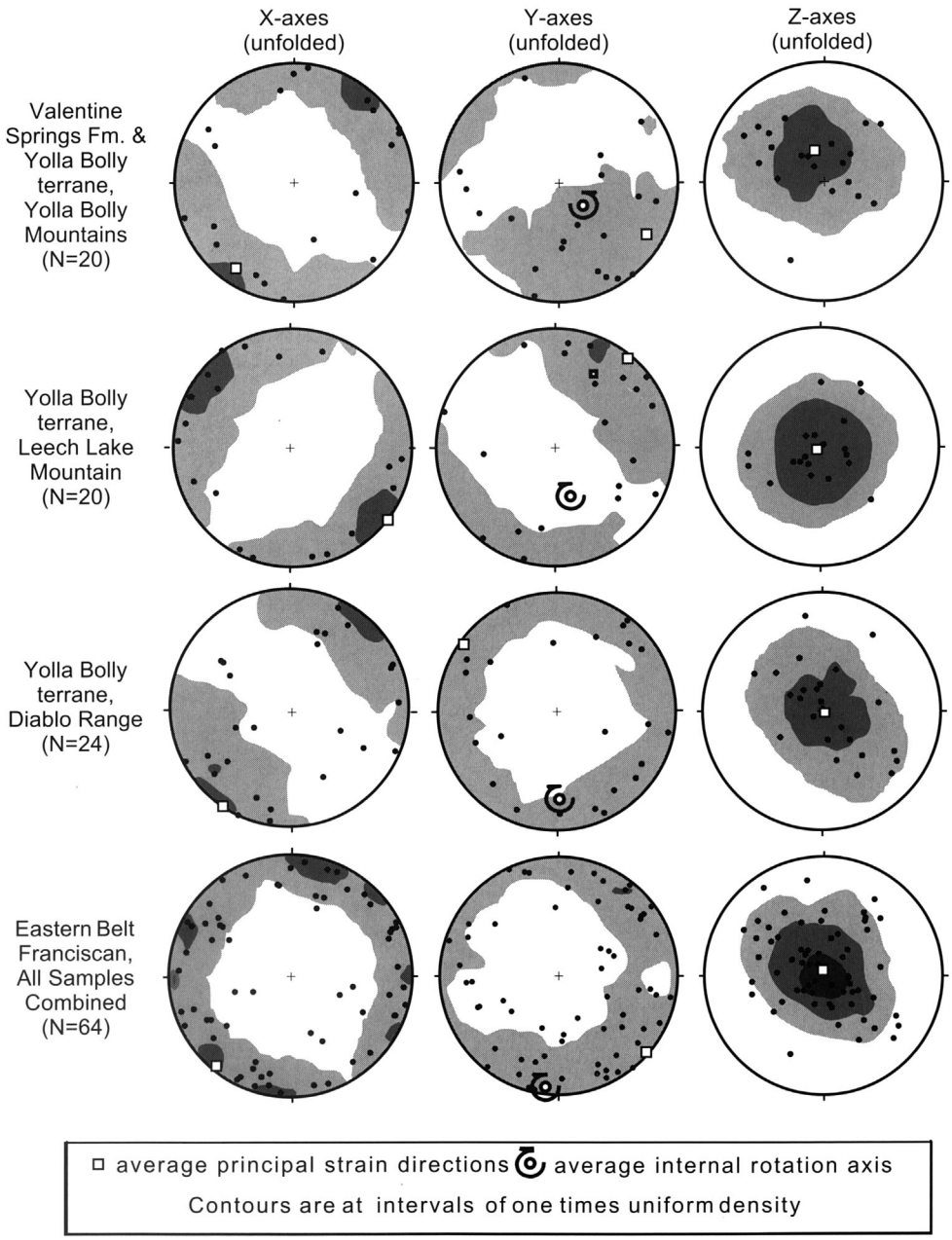

Fig. 7. Lower-hemisphere equal-area stereograms for 'unfolded' principal stretch directions in the Yolla Bolly Mountains, at Leech Lake Mountain, in the Diablo Range, and for all data combined. Also shown are axes and relative shear sense for the tensor-averaged internal rotations. Contours were determined using the method of Kamb (1959) and are shown at intervals of one times uniform density.

determined separately using the Hencky and velocity-gradient methods, respectively (see Appendix B of Brandon (1995) for details about methods).

The measurements in Table 4 and Fig. 7 have been adjusted for the effects of broad folding, probably late Cenozoic in age. Apatite fission-track cooling ages (Dumitru 1989) indicate that

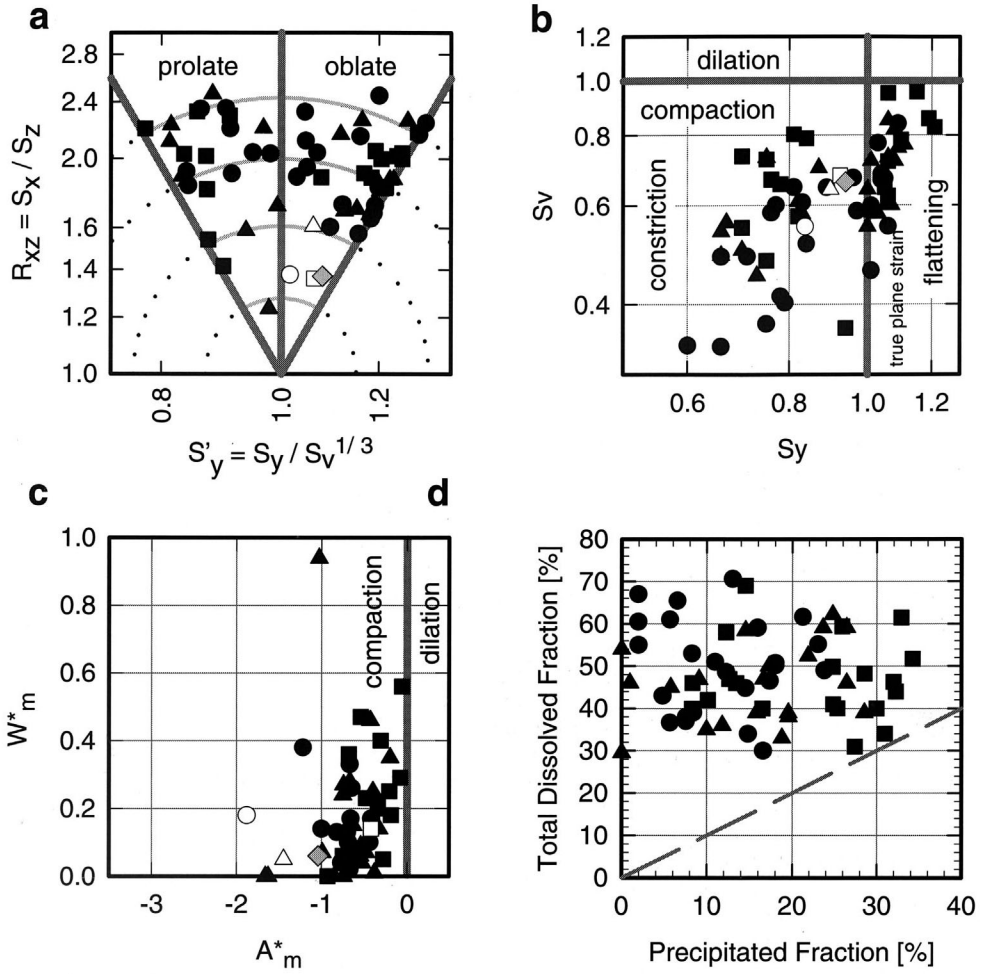

Fig. 8. Graphical summary of deformation data. Plots symbols are: squares for Yolla Bolly Mountain study area, triangles for Leech Lake Mountain, and circles for Diablo Range. Open symbols show averages for each study area. Grey diamond shows grand mean for all data. (**a**) Nadai plot showing strain symmetry and deviatoric strain magnitude (Brandon 1995). Circular contours mark 0.2 increments of octahedral shear strain, a measure of deviatoric strain magnitude. The data indicate both oblate and prolate symmetries. (**b**) Strain type, as indicated by the $S_V - S_Y$ plot of Brandon (1995). Note that the individual measurements fall mainly in the constrictional field, but the tensor averages plot near the plane strain boundary. (**c**) Plot of the kinematic vorticity number versus the kinematic dilatancy number. (**d**) Total percentage of dissolved grain mass versus percentage precipitated as fibre overgrowths. The difference between these two measures indicates the amount of grain mass removed from the rock.

the sampled rocks were at less than *c.* 3 km depth during much of Cenozoic time. We infer that, at shallow depths, Cenozoic folding would have been accommodated by flexural slip on discrete surfaces. Thus, sandstone units would be expected to have rotated in a rigid fashion as limb dip increased. To restore the effects of this young and relatively modest deformation, we have estimated the geometry and limb angles associated with regional-scale folds in our study areas. The measured principal directions for each sample were then rotated about the fold axis and by the amount of local limb dip. For the Yolla Bolly and Leech Lake areas, the average fold axis of broad regional antiforms and synforms (Fig. 4) has a trend and plunge of 120° and 20°. Restoration of limb dips required between 10° and 30° of rotation around this fold axis. The overall structure of the Diablo Range is more complicated, with a number of variably oriented

antiforms and synforms which mainly trend 140–160° with a plunge of 10–20°. In rare cases, the folds trend 100–110° with plunges of 10–20°. Restoration of limb dips involve 10–40° rotation about these fold axes. The corrected data are designated as 'unfolded' in Tables 4 and 5, whereas the original, uncorrected data are designated as 'present coordinates' (Tables 3 and 5). In most cases, the 'unfolding' correction produces only a modest change in the orientation of the individual measurements. Tensor averages for each study area (Table 5) are also little affected by the 'unfolding' corrections.

Finite strain

Yolla Bolly Mountains. The field orientations of the measured finite-strain axes show scattered orientations (Fig. 4, Table 3). In the Yolla Bolly terrane, cleavage typically has a moderate dip and a variable strike. X generally plunges gently within the cleavage plane. Stereograms of 'unfolded' principal directions (Fig. 7) reveal a well-defined subvertical maximum for Z and a subhorizontal girdle for X with maxima plunging gently to the NE and SW. The maxima in the stereograms have similar orientations to the principal directions of the average strain tensor (Table 5), which are shown as open squares in Fig. 7.

Modes indicate that the sandstones are made up of 3–34% fibre by volume. S_X shows a relatively wide scatter, ranging from 1.06 to 1.52. S_Z ranges from 0.53 to 0.77, and S_Y ranges from 0.70 to 1.19 with the data split evenly between constrictional ($S_Y < 1$) and flattening ($S_Y > 1$) strain types (Fig. 8b). The tensor average (S_X:S_Y:S_Z = 1.02:0.96:0.75, Table 5) indicates little shortening in X and Y at the regional scale. What may seem odd about this result is that the tensor average for S_X falls outside the range of individual S_X values. The reason is that the individual strain tensors do not share the same principal directions. In particular, because X and Y are variable at the local scale, local variations in S_X and S_Y tend to be averaged out, which accounts for why the tensor averages for S_X and S_Y are *c.* 1.

The principal directions for sandstones from the Valentine Springs Formation of the Pickett Peak terrane are similar to those from the Yolla Bolly terrane (Fig. 4, Tables 3 and 4), but the tensor average (S_X:S_Y:S_Z = 1.16:0.86:0.53, Table 5) indicates smaller S_Y and S_Z values and a slightly larger S_X value.

Leech Lake Mountain. The field orientations of the finite-strain axes and the orientation of cleavage are similar to those in the Yolla Bolly Mountains (Fig. 5, Table 3). The only difference is that the average X is horizontal in a NW–SE direction, as indicated by the tensor average and the stereograms (Table 5, Fig. 7). Fibre modes for individual samples are between 0% and 29%, with three samples lacking fibres at all. The absolute stretches range from 1.00 to 1.36 for S_X, 0.66 to 1.09 for S_Y, and 0.50 to 0.81 for S_Z. The tensor average is S_X:S_Y:S_Z = 1.06:0.91:0.66 (Table 5).

Diablo Range. The field orientations of the finite-strain axes and the cleavage attitudes resemble those in the Yolla Bolly Mountains and at Leech Lake Mountain (Fig. 6, Table 3). This area is similar to the Yolla Bolly Mountains in that the average X is horizontal in a NE–SW direction (Table 5, Fig. 7). Fibre modes for individual samples are between 2% and 23%. Absolute stretches for S_X range from 1.01 to 1.30. S_Y is once again both constrictional and flattening (Fig. 8b) with values ranging from 0.60 to 1.09. S_Z ranges from 0.45 to 0.70. The tensor average gives principal stretches of S_X:S_Y:S_Z = 0.95:0.83:0.69.

All areas combined. The tensor averages indicate that SMT deformation at the regional scale was similar in all three study areas. This result is remarkable given that the study areas are spaced over a distance of *c.* 500 km along the Franciscan margin. The grand tensor average for all strain measurements gives S_X:S_Y:S_Z = 0.96:0.92:0.70 (Table 5), which indicates contraction in Z but almost no strain in X and Y. This deformation is best viewed as plane strain uniaxial shortening, with the shortening in Z balanced by a comparable mass-loss volume strain. The average Z direction is subvertical and indicates moderate vertical thinning of the wedge.

Volume strain

All Eastern Belt sandstones show significant compactional volume strains, ranging from 4% to 66% with an average of 38% (Table 5). We reiterate that these measurements represent mass-loss volume strains, because they are defined by the difference between the loss of mass from the detrital grains and the precipitation of new mass in the fibre overgrowths (Fig. 8d). As noted above, other sources of volume strain, such as changes in porosity or average mineral density, are considered to have been unimportant during SMT deformation and to have had no significant influence on our PDS and mode measurements. Our modal measurements provide a complete inventory of the

volume of grains, selvage, and fibre in each sample. Thus, we contend that the missing mass has moved beyond the scale of an individual rock sample.

At the outcrop scale, there is no evidence of a sink for this missing mass. Modal measurements performed at Leech Lake Mountain along line traverses across outcrops show that veins make up no more than 3% by volume of a typical outcrop with the average about 1%. We conclude that SMT deformation was accomplished by a relatively large flux of fluid that was able to dissolve the grains and transport the dissolved load over great distances (several kilometres and perhaps more). Work in progress in the Central and Coastal Belts of the Franciscan indicates that the missing mass was not precipitated there. This leaves us with two options: either the missing mass was precipitated at a deeper level within the wedge, or it left the wedge entirely, perhaps carried by fluids that were vented on the sea floor or subducted into the mantle.

SMT deformation included both closed and open exchange involving local precipitation of fibre overgrowth and wholesale loss of mass from the rock (Fig. 8d). The open-system exchange was apparently controlled by dissolution and removal of the more soluble components of the rock. In contrast, the closed-system exchange was controlled by grain-scale transport of the relatively insoluble components of the rock. The presence of relatively Al-rich phases in the fibre overgrowths, such as phengite, chlorite, and lawsonite, is consistent with the very low solubility of Al species in a normal metamorphic fluid. Thus, the growth of the extensional fibres is probably well approximated by the closed-system Coble creep mechanism (Elliott 1973), whereas the mass-loss volume strain must be related to the dissolution and transport properties of an advecting fluid.

Internal rotation

For individual samples, the measured internal rotation axis is commonly subparallel to Y (Table 3). The rotation axes vary considerably at the local scale and show no systematic patterns in map view. Their distribution is similar to that observed for the Y directions. Internal rotation angles are generally small, with $\Omega_i < 10^\circ$ in all but two samples. Individual measurements of W^*_m are generally <0.4 (Table 3; Fig. 8c).

The tensor-averaged internal rotation axes (Table 5; centre stereograms in Fig. 7) show considerable variation between the study areas. Furthermore, there is no longer any parallelism between the rotation axes and Y. These results might be due to the fact that the average internal rotation angles and kinematic vorticity numbers for the study areas are very small, with $\Omega_i < 3^\circ$ and $W^*_m < 0.26$ (Table 5). The main conclusion is that SMT deformation in the Eastern Belt sandstones was close to coaxial, both at the local and regional scale.

Discussion

Our study provides only a preliminary view of deformation in the Franciscan wedge. None the less, it challenges many first-order predictions about deformation in accretionary wedges. Cloos & Shreve (1988) argued that subduction-related accretionary wedges are dominated by a strongly shearing flow, but our results show only low-magnitude coaxial deformation. Almost all wedge models assume isochoric deformation, which forces a balance between shortening and extension, but our results indicate that mass-loss volume strains are an integral part of the deformation. It is commonly inferred that dislocation glide becomes important in wedges that are thicker than about 15 km (Davis *et al.* 1983; Pavlis & Bruhn 1983) but our observations indicate that the SMT mechanism remained the dominant ductile deformation mechanism to depths of 25–30 km in the Franciscan wedge. Wakabayashi (1992) has argued that margin-parallel linear fabrics in the Franciscan Complex might have been produced by oblique convergence but our results indicate that when averaged at the regional scale, margin-parallel ductile strains are close to zero.

Issues that remain unresolved in our study include the role of shear partitioning, either as spin of beds or blocks or as enhanced non-coaxial deformation in mudstone-rich units. The sandstone units that we have sampled show no evidence of large spin-induced rotations (i.e. rigid rotations). We have no quantitative information about deformation in mudstone lithologies, which occur as interbeds in turbidite sequences and in local mélange units. We note, however, that mudstones typically make up less than 40% of the Eastern Belt, and are even less common in the Yolla Bolly terrane, which is dominated in many places by massive sandstones. Mudstones of the Eastern Belt do not show any unusually strong fabrics, which suggests that the degree of deformation is not greatly different from that measured in the sandstones. Furthermore, the mudstones do not appear to be unusual in composition, which might be the case if the mass dissolved from the sandstones was precipitated in adjacent mudstone units. These issues are being addressed by

work in progress, but nothing has been found yet to suggest that our preliminary inferences here are incorrect.

Ductile fabrics at Del Puerto Canyon

We have already outlined the proposal of Platt (1986) that the Eastern Belt was exhumed by normal slip on the Coast Range fault zone. Subsequent work has indicated that much of what we now see as the Coast Range fault zone formed during Cenozoic time above an eastward-moving tectonic wedge or triangle zone (Wentworth *et al.* 1984; Glen 1990; Unruh *et al.* 1995; Wakabayashi & Unruh 1995).

Harms *et al.* (1992) proposed that the Del Puerto area (Fig. 6) might preserve an older record of Coast Range faulting because the gentle dip of the fault zone at Del Puerto indicated that it was little affected by Cenozoic tectonic wedging. Harms *et al.* (1992) reported the presence of a 'mylonitic lineation' in Yolla Bolly terrane sandstones exposed directly below the Coast Range fault zone at Del Puerto Canyon (Fig. 6). They argued that an anastomosing SMT cleavage present in the sandstone was analogous to S–C fabrics typically found in high-temperature metamorphic rocks (Berthé *et al.* 1979). The direction and sense of shear inferred from this fabric were variable (fig. 3 in Harms *et al.* 1992): out of a total of 22 measurements, 13 were top-east, seven top-west, and two top-north. The predominance of top-east indicators was taken as evidence for a normal sense of shear within the easternmost Franciscan Complex and, by inference, across the Coast Range fault zone as well. This interpretation predicts strong non-coaxial ductile deformation within the easternmost Franciscan Complex.

We were not able to directly sample the S–C fabrics of Harms *et al.* (1992) because of private property restrictions. None the less, some of our samples are from Del Puerto Canyon (Fig. 6) and at least one is adjacent to or within the proposed ductile shear zone. We did not see any mylonitic rocks in the field, and low strain magnitudes indicate that none of our samples from Del Puerto Canyon and adjacent areas have a mylonitic fabric (see Nos 41–56 in Table 3). The strain results do indicate large local variations in X in the Del Puerto area (Fig. 6). Internal rotation axes are also variable in orientation, but ductile deformation appears to have been approximately coaxial ($W^*_m < 0.35$). Linear fabrics are present at the local scale, but our tensor-averaged results indicate that there was little to no extension associated with regional-scale ductile deformation (see Yolla Bolly terrane, Mount Hamilton area, in Table 5). Deformation measurements for rocks containing the S–C fabrics of Harms *et al.* (1992) are needed before this problem can be fully resolved. However, at present, our deformation measurements are difficult to reconcile with the interpretation of a normal-sense ductile shear zone within the easternmost Franciscan Complex.

Viscous versus Coulomb wedges

Our results do not provide a definitive test of Platt's (1986) viscous wedge model but they do help to characterize the nature and magnitude of ductile flow within the Franciscan wedge. We have shown that strain magnitudes were low, despite the relatively deep accretion and long residence time of the Eastern Belt rocks. The largest strains are in the Z direction and indicate an average of *c.* 30% shortening. Assuming a coaxial deformation and residence times of 60–30 Ma, these shortening strains would require average strain rates of (2 to 4) $\times 10^{-16}$ s^{-1}, which is 2–25 times slower than the 10^{-14} s^{-1} strain rates anticipated by Platt (1986). This comparison is crude, and ignores the fact that strain rates are clearly not uniform throughout the wedge. None the less, the point we want to emphasize is that the magnitudes of SMT strains in the Franciscan wedge are fairly small. From this we infer that the stability of the Franciscan wedge is probably better represented by the Coulomb wedge criterion than by a viscous wedge criterion as advocated by Platt (1986). We infer that the SMT mechanism operated as a background deformation process. Ductile strains were fast enough and residence times long enough for the rocks to develop a fabric, but they were probably too slow to significantly influence the stability of the wedge.

Platt (1986) argued that underplating could drive the upper part of a viscous Franciscan wedge into extensional failure which would allow syn-convergent tectonic exhumation. This interpretation, however, is probably only tenable for a viscous wedge. Dahlen (1984) showed that accretion alone was not capable of driving a convergent Coulomb wedge from a thrust-dominated taper (Region I in the taper stability plot of Dahlen (1984)) to a taper where normal faults are active (Regions II and III of Dahlen (1984)). Such a transition would require a significant decrease in dip and/or strength of the décollement. Krueger & Jones (1989) and Harms *et al.* (1992) have argued that the transition to a shallowly subducting slab during the Laramide orogeny might have triggered extensional failure

of the Franciscan wedge. The décollement dip for modern accretionary wedges is generally <8° (Davis *et al.* 1983). Thus, the amount of rotation of the wedge caused by shallowing of the Laramide slab was probably <8°. This amount of rotation would not be sufficient to cause extensional failure in a Coulomb wedge unless the décollement was very weak (Dahlen 1984). A weak décollement might result from high pore fluids at the base of the wedge or rheological changes, such as the thermal activation of dislocation-controlled ductile flow (Pavlis & Bruhn 1983).

Exhumation by ductile thinning

Ductile deformation may not have been an important factor in controlling the stability of the Franciscan wedge, but ductile thinning did contribute to exhumation. Feehan & Brandon (1999) introduced a one-dimensional steady-state model to estimate the contribution of ductile deformation to exhumation of a generic accretionary wedge (Fig. 9). The model tracks the vertical progress of a material point through a steady-state wedge from its site of initial accretion at depth z_b to its exhumation at the surface of the wedge at $z = 0$. Ductile thinning is defined as the change in thickness of the overburden above a material point because of ductile deformation within the overburden. To estimate the contribution of ductile thinning to exhumation, it is necessary to specify $\boldsymbol{L}(z)$, which is the velocity-gradient tensor as a function of depth. Ductile SMT deformation is considered to be the primary deformation mechanism that operated within the Franciscan wedge. Based on the simple coaxial fabrics observed in our samples, we infer that the principal strain rates for SMT deformation remained constant in direction and polarity throughout the wedge. To mimic this condition, $\boldsymbol{L}(z)$ is scaled so that its components increase linearly with depth. As discussed by Feehan & Brandon (1999), a rheologically based rate law would be preferable but one is not available. A depth-proportional relationship provides a reasonable first-order approximation given that silica solubility, mean effective stress, and deviatoric stress are all expected to increase with depth.

The kinematic model assumes a steady-state wedge, where the rates of basal accretion $\dot{a}$, ductile deformation $\boldsymbol{L}(z)$, and near-surface exhumation caused by erosion $\dot{\varepsilon}$ and shallow normal faulting $\dot{\eta}$ all remain constant with time (Fig. 9). If the steady-state assumption were correct, then all material points within the overburden would have experienced the same deformation history as the material point being tracked. We can solve for specific values for $\boldsymbol{L}(z)$ given the fact that integration of $\boldsymbol{L}(z)$ along the material path through the wedge should give the finite strain and internal rotation measured in exhumed rocks. The EXHUME program (Feehan & Brandon 1999) was used to calculate results reported here.

It is difficult to evaluate if and when the Franciscan wedge achieved a steady-state configuration, defined by an accretionary flux into the wedge equal to the erosional flux out of the

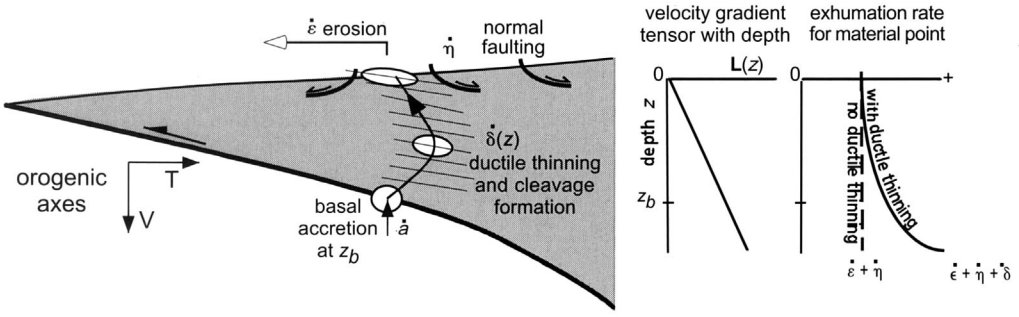

Fig. 9. Exhumation model of Feehan & Brandon (1999) illustrating the relationship between basal accretion, ductile flow, and exhumation in a steady-state wedge. A particle enters the base of the wedge at z_b, where it starts to deform in a ductile manner as it moves upward through the wedge. The rate of basal accretion is indicated by $\dot{a}$, and the deformation rate along the exhumation path is represented by the velocity gradient tensor $\boldsymbol{L}(z)$, which is assumed to increase linearly with z. The rate of exhumation, which changes along the exhumation path, is equal to the sum of the rate of ductile thinning of the overlying cover $\dot{\delta}(z)$, and rate of thinning by shallow normal faulting $\dot{\eta}$, and the erosion rate $\dot{\varepsilon}$. The model assumes a steady-state wedge, where accretion, ductile flow, erosion and normal faulting remain constant with time. Orogenic axes T and V indicate the across-strike and vertical directions, respectively.

forearc high. The general inference is that an accretionary wedge will gradually approach a steady-state configuration as long as the rate of accretion and the internal state of the wedge remain fairly constant with time. As an example, Brandon *et al.* (1998) estimated that about 20–50 Ma are needed to achieve a steady-state configuration at the Cascadia accretionary wedge.

Our strain results indicate that the horizontal strain rate through the Franciscan wedge was probably contractional throughout the entire wedge. In this case, the only way that the wedge could have reached a steady state would have been by emergence and erosion of the forearc high. Sedimentological data indicate strong uplift on the west side of the Great Valley basin starting at 84–75 Ma (Moxon & Graham 1987; Moxon 1988). We have already summarized evidence that uplift and exhumation in the Franciscan forearc high had brought the Eastern Belt to the surface by Paleocene time (66–55 Ma) (e.g. Berkland 1973). Therefore, we infer that the Franciscan forearc high became emergent sometime in latest Cretaceous time, but no earlier than *c.* 84 Ma. By then, the accretionary wedge had been growing for some 75 Ma. If the wedge was exhumed mainly by erosion, then it seems likely that it reached a steady state during latest Cretaceous and early Tertiary time. To be consistent with our steady-state assumption, we limit our analysis here to the Yolla Bolly terrane, which was accreted and exhumed during this period of time.

To solve for the best-fit parameters, the EXHUME program iterates through a series of guesses to find parameters that give the observed amount of exhumation and finite strain (see Feehan & Brandon (1999) for details of best-fit calculation). Residence time and depth of accretion are taken from Table 1. The tensor averages in Table 5 are used to represent the ductile deformation. The results of the calculation (Table 6; Fig. 10) indicate that ductile strain contributed about 8–13% to the overall exhumation. This low value reflects the fact that ductile strains are fastest at depth as prescribed by the depth-proportional relationship for $\boldsymbol{L}(z)$. The contribution would be even less if $\boldsymbol{L}(z)$ increased nonlinearly with depth. Conversely, a constant $\boldsymbol{L}(z)$ would give the largest contribution, about 12–19%, but such a constant deformation rate with depth seems unlikely.

Thus, we conclude that ductile thinning accounts for only about *c.* 3 km of the exhumation of the Eastern Belt. The remaining *c.* 24 km must have been accommodated by some other process such as normal faulting or erosion. We have already noted that there is no direct evidence for normal faulting in the Franciscan Complex. Thus, we suggest that erosion might have been the dominant exhumation process. The predicted rates, *c.* 0.4–0.8 km Ma^{-1}, are not unusual for erosion of an emergent forearc high. For instance, Brandon & Vance (1992) and Brandon *et al.* (1998) estimated that the long-term erosion rate for the Olympic Mountains segment of the Cascadia forearc high ranged from 0.3 to 0.75 km Ma^{-1}. By analogy to the Olympic Mountains, we envision that most of the sediments eroded from the Franciscan forearc high were transported to the west and redeposited in trench-slope basins and in the trench itself (Ring & Brandon 1994). This would account for why there is so little evidence in the Great Valley basin for deep erosion of the forearc high (Wakabayashi & Unruh 1995).

The model calculation also provides vertically averaged ductile strain rates parallel to the principal directions of the Franciscan wedge (*T*, *P*, and *V* in Table 7). We can use these values to make a rough estimate of how much plate

Table 6. *Results of exhumation calculations for the Yolla Bolly terrane using a depth-dependent rate for ductile deformation*

Study areas	Rates (km Ma^{-1})			Integrated values		
	$\dot{a}$	$\dot{\delta}(z_b)$	$\dot{\varepsilon}+\dot{\eta}$	δ (km)	$\varepsilon+\eta$ (km)	$\frac{\delta}{(\delta+\varepsilon+\eta)}$ (%)
Yolla Bolly Mountains	0.54	0.12	0.42	2.2	23.8	8
Leech Lake Mountain	0.59	0.20	0.39	3.5	22.5	13
Diablo Range	1.10	0.33	0.73	3.3	24.7	12

$\dot{a}$, basal accretion rate; $\dot{\delta}(z_b)$, vertical ductile thinning rate for a point at depth z_b, the base of the wedge; $\dot{\varepsilon}+\dot{\eta}$, combined exhumtion rates for erosion $\dot{\varepsilon}$ and normal faulting $\dot{\eta}$; δ, amount of exhumation caused by vertical ductile thinning; $\varepsilon+\eta$, amount of exhumation caused by erosion ε and shallow normal faulting η; $\delta+\varepsilon+\eta$, total exhumation; $\delta/(\delta+\varepsilon+\eta)$, relative contribution of ductile thinning to exhumation.

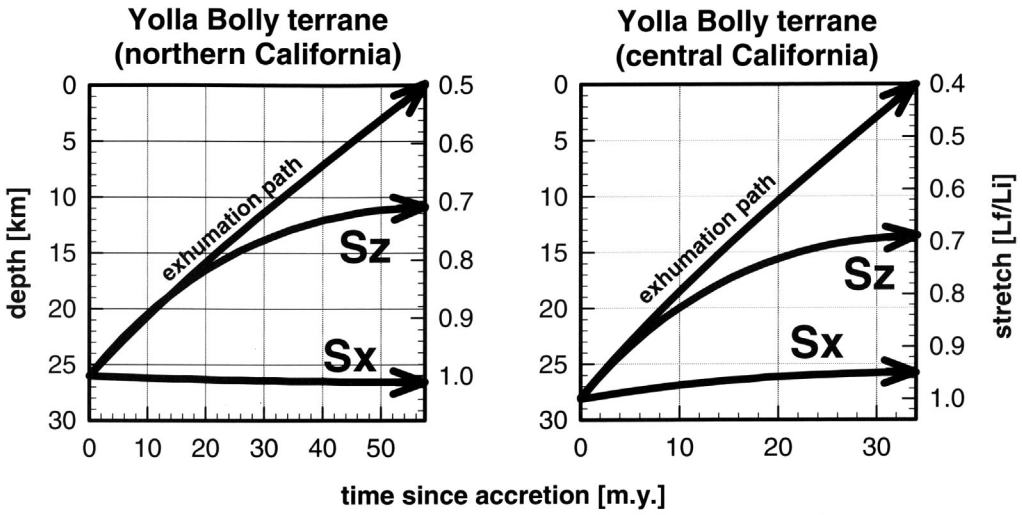

Fig. 10. Strain and exhumation paths estimated for the Yolla Bolly terrane. For this calculation, the rate of ductile deformation was assumed to increase linearly with depth. See Tables 6 and 7 for numerical results.

Table 7. *Strains and vertically averaged strains rates for SMT deformation in the Yolla Bolly terrane*

Unit and study area	Across-strike (*T*)	Parallel-to-strike (*P*)	Vertical (*V*)
Yolla Bolly terrane,	+0%	–6%	–23%
Yolla Bolly Mtns	$+4 \times 10^{-18}$ s^{-1}	-4×10^{-17} s^{-1}	-2×10^{-16} s^{-1}
Yolla Bolly terrane,	–6%	+2%	–34%
Leech Lake Mtn	-4×10^{-17} s^{-1}	$+2 \times 10^{-17}$ s^{-1}	-2×10^{-16} s^{-1}
Yolla Bolly terrane,	–8%	–15%	–31%
Diablo Range	-8×10^{-17} s^{-1}	-2×10^{-16} s^{-1}	-4×10^{-16} s^{-1}

Strains and strain rates were calculated using averages from Table 5 for 'unfolded' data and assuming a depth-dependent deformation rate. Maximum strain rates would be twice the vertically averaged rates given here. Average strike of Franciscan wedge is about 155°.

convergence was accommodated by ductile deformation within the Franciscan wedge. The average across-strike strain rate indicates a horizontal shortening rate <0.25% Ma^{-1} (*T* in Table 7). This upper bound probably holds for the more outboard part of the wedge, which was thinner and cooler, and therefore should have had even lower rates of ductile shortening. The width of the actively deforming accretionary wedge was probably <200 km. Thus, the rate of convergence accommodated by within-wedge ductile flow was probably <0.5 km Ma^{-1}. Convergence rates at the Franciscan margin were about 100 km Ma^{-1} (Engebretson *et al.* 1985), which means that *c.* 6000 km of oceanic crust would have been subducted in 60 Ma. Our estimates suggest that <30 km of this convergence was accommodated by within-wedge ductile deformation. From this we infer that the wedge remained largely decoupled from the subducting plate. The fact that rocks within the wedge were able to form significant ductile fabrics is due to their long residence time in the wedge.

Conclusions

This paper presents the first comprehensive study of ductile deformation in the Franciscan wedge. The Franciscan Complex is often considered to be the prototypical sediment-rich accretionary wedge and therefore our results should have broad implications for other subduction-related wedges. Our major conclusions are as follows:

(1) Ductile deformation was slow within the Franciscan wedge, probably because of the low thermal gradients that typify this setting. SMT was the most active ductile mechanism and

appears to have remained so to depths of 25 and 30 km. Even so, the slow rates for SMT deformation indicate that it operated as a background deformation process and probably had little influence on the stability of the wedge.

(2) At the regional scale, SMT deformation was characterized by uniaxial vertical shortening with little to no strain in the horizontal. Vertical shortening was accommodated by a pervasive mass-loss volume strain, averaging about 38%. There is no evidence of where the dissolved mass went, so we are forced to consider large-scale transport by an advecting fluid. Unlike many other strain studies, our methods have allowed us to measure absolute strains associated with SMT deformation. As a result, our estimates of mass-loss volume strains are based on direct measurements and cannot be easily dismissed. The reliability of our results are supported by their consistency over such a large region of the Eastern Belt, and by the fact that tensor averages for each study area indicate a deformation that is consistent with plane strain across the Franciscan wedge.

(3) Within-wedge ductile deformation was nearly coaxial at the regional scale. This result poses a serious challenge for geodynamic models that postulate strongly shearing flows within the wedge or for tectonic models that advocate normal-sense ductile shear zones along the eastern side of the Franciscan wedge.

(4) Ductile thinning can account for about 10% of the exhumation of the Eastern Belt rocks. The remaining *c.* 24 km of exhumation is attributed to erosion of an emergent forearc high. We show that the inferred rates of erosion, between 0.4 and 0.8 km/ Ma^{-1}, are reasonable when compared with modern erosion rates for the Cascadia forearc high.

This work was supported by National Science Foundation grants EAR9005777, EAR9305367, and INT9513911 to M.T.B., and a Feodor-Lynen fellowship from the Alexander von Humboldt-Stiftung and grant Ri538/8–1 from the Deutsche Forschungsgemeinschaft to U.W. We thank R. Bolhar in particular for letting us use data on Leech Lake Mountain from his Diploma thesis. J. Wakabayashi kindly provided invaluable information about various details of Franciscan geology. We thank the two anonymous referees and associate editor S. Willett for thoughtful reviews.

References

BAILEY, E. H., IRWIN, W. P. & JONES, D. L. 1964. Franciscan and related rocks, and their significance in the geology of western California. *California Division of Mines and Geology Bulletin*, **183**, 1–177.

BAUDER, J. M. & LIOU, J. G. 1979. Tectonic outlier of Great Valley sequence in Franciscan terrane, Diablo Range, California. *Geological Society of America Bulletin*, **90**, 561–568.

BERKLAND, J. O. 1973. Rice Valley Outlier, new sequence of Cretaceous–Paleocene strata in northern Coast Ranges, California. *Geological Society of America Bulletin*, **84**, 2389–2405.

——, RAYMOND, L. A., KRAMER, J. C., MOORES, E. M. & O'DAY, M. 1972. What is Franciscan? *Bulletin, American Association of Petroleum Geologists*, **56**, 2295–2302.

BERTHÉ, D., CHOUKROUNE, P. & JEGUZO, P. 1979. Orthogneiss, mylonite and non-coaxial deformation of granites. *Journal of Structural Geology*, **1**, 31–42.

BLAKE, M. C., JR, JAYKO, A. S., MCLAUGHLIN, R. J. & UNDERWOOD, M. B. 1988. Metamorphic and tectonic evolution of the Franciscan Complex, northern California. *In*: ERNST, W. G. (ed.) *Metamorphism and Crustal Evolution of the Western United States*. Prentice–Hall, Englewood Cliffs, NJ, 1036–1059.

BOLHAR, R. 1997. *Absolute strain analysis of metasediments from the Franciscan subduction complex, Californian Coast Ranges*. Diploma thesis, Universität Mainz.

BRANDON, M. T. 1995. Analysis of geologic strain data in strain–magnitude space. *Journal of Structural Geology*, **17**, 1375–1385.

—— & VANCE, J. A. 1992. Tectonic evolution of the Cenozoic Olympic subduction complex, Washington State, as deduced from fission track ages for detrital zircons. *American Journal of Science*, **292**, 565–636.

——, COWAN, D. S. & FEEHAN, J. G. 1994. Fault-zone structures and solution-mass-transfer cleavage in Late Cretaceous nappes, San Juan Islands, Washington. *In*: SWANSON, D. A. & HAUGERUD, R. A. (eds.) *Geologic Field Trips in the Pacific Northwest*. Geological Society of America Annual Meeting, Seattle, WA, 1994, 2L, 1–19.

——, RODEN-TICE, M. K. & GARVER, J. I. 1998. Late Cenozoic exhumation of the Cascadia accretionary wedge in the Olympic Mountains, NW Washington State. *Geological Society of America Bulletin*, **110**, 985–1009.

BRÖCKER, M. & DAY, H. W. 1995. Low-grade blueschist facies metamorphism of metagreywackes, Franciscan Complex, northern California. *Journal of Metamorphic Geology*, **13**, 61–78.

CHAPPLE, W. M. 1978. Mechanics of thin-skinned fold-and-thrust belts. *Geological Society of America Bulletin*, **89**, 1189–1198.

CHESTERMAN, C. W. 1963. Intrusive ultrabasic rocks and their metamorphic relationships at Leech Lake Mountain: Mendocino County, California. *California Division of Mines and Geology Bulletin*, **82**, 5–10.

CHOPIN, C. 1984. Coesite and pure pyrope in high-grade blueschists of the Western Alps; a first record and some consequences. *Contributions to Mineralogy and Petrology*, **86**, 107–118.

CLOOS, M. & SHREVE, R. 1988. Subduction-channel model of prism accretion, melange formation, sediment subduction, and subduction erosion at

convergent plate margins: 2. Implications and discussion. *Pageoph*, **128**, 501–545.

COLEMAN, R. G. & LANPHERE, M. A. 1971. Distribution and age of high-grade blueschists, associated eclogites, and amphibolites from Oregon and California. *Geological Society of America Bulletin*, **82**, 2397–2412.

—— & WANG, X. 1995. *Ultrahigh Pressure Metamorphism*. Cambridge University Press, Cambridge.

COWAN, D. S. 1974. Deformation and metamorphism of the Franciscan subduction zone complex northwest of Pacheco Pass, California. *Geological Society of America Bulletin*, **85**, 1623–1634.

—— & BRUHN, R. L. 1992. Late Jurassic to early Late Cretaceous geology of the U.S. Cordillera. *In*: BURCHFIEL, B. C. *et al.* (eds) *The Cordilleran Orogen: Conterminous US*. Geological Society of America, Geology of North America, Boulder, CO, **G-3**, 169–203.

—— & PAGE, B. M. 1975. Recycled material in Franciscan melange west of Paso Robles, California. *Geological Society of America Bulletin*, **86**, 1089–1095.

COX, A. & HARTE, R. B. 1986. *Plate Tectonics*. Blackwell, Oxford.

DAHLEN, F. A. 1984. Noncohesive critical Coulomb wedges: an exact solution. *Journal of Geophysical Research*, **89**, 10125–10133.

DAVIS, D., SUPPE, J. & DAHLEN, F. A. 1983. Mechanics of fold-and-thrust belts and accretionary wedges. *Journal of Geophysical Research*, **88**, 1153–1172.

DEWEY, J. F. 1988. Extensional collapse of orogens. *Tectonics*, **7**, 1123–1140.

DICKINSON, W. R., INGERSOLL, R. V., COWAN, D. S., HELMOLD, K. P. & SUCZEKI, C. A. 1982. Provenance of Franciscan greywackes in coastal California. *Geological Society of America Bulletin*, **93**, 95–107.

——, OJAKANGAS, R. W. & STEWART, R. J. 1969. Burial metamorphism of the late Mesozoic Great Valley sequence, Cache Creek, California. *Geological Society of America Bulletin*, **80**, 519–526.

DUMITRU, T. A. 1989. Constraints on uplift in the Franciscan Subduction Complex from apatite fission track analysis. *Tectonics*, **8**, 197–220.

DURNEY, D. W. & RAMSEY, J. G. 1973. Incremental strains measured by syntectonic crystal growths. *In*: DEJONG, K. A. & SCHOLTEN, R. (eds) *Gravity and Tectonics*. Wiley, New York, 67–96.

EFRON, B. 1982. *The Jackknife, the Bootstrap, and other Resampling Methods*. CBMS–NSF Regional Conference Series in Applied Mathematics, Society for Industrial and Applied Mathematics, Philadelphia, PA.

ELLIOTT, D. 1973. Diffusion flow laws in metamorphic rocks. *Geological Society of America Bulletin*, **84**, 2645–2664.

ELLIS, M. A. 1986. The determination of progressive deformation histories from antitaxial syntectonic crystal fibres. *Journal of Structural Geology*, **8**, 701–710.

ENGEBRETSON, D. G., COX, A. & GORDON, R. C. 1985. *Relative motions between oceanic and continental plates in the Pacific basin*. Geological Society of America, Special Papers, **206**.

ENGLAND, P. C. & RICHARDSON, S. W. 1977. The influence of erosion upon the mineral facies of rock from different metamorphic environments. *Journal of the Geological Society, London*, **134**, 201–213.

ERNST, W. G. 1965. Mineral parageneses in Franciscan metamorphic rocks, Panoche Pass, California. *Geological Society of America Bulletin*, **76**, 879–914.

—— 1987. Jadeitized Franciscan metamorphic rocks of the Pacheco Pass–San Luis Reservoir area, central California Coast Ranges. *Geological Society of America Centennial Field Guide – Cordilleran Section*, **57**, 245–250.

—— 1992. Response to R.H. Grapes. *New Zealand Journal of Geology and Geophysics*, **35**, 385–387.

—— 1993. Metamorphism of Franciscan tectonostratigraphic assemblage, Pacheco Pass area, east-central Diablo Range, California Coast Ranges. *Geological Society of America Bulletin*, **105**, 618–636.

FASSOULAS, C., KILIAS, A. & MOUNTRAKIS, D. 1994. Postnappe stacking extension and exhumation of high-pressure/low-temperature rocks in the island of Crete, Greece. *Tectonics*, **13**, 127–138.

FEEHAN, J. G. & BRANDON, M. T. 1999. Contribution of ductile flow to exhumation of low T – high P metamorphic rocks: San Juan – Cascade Nappes, NW Washington State. *Journal of Geophysical Research*, in press.

FISHER, D. M. & BRANTLEY, S. L. 1992. Models of quartz overgrowth and vein formation: deformation and episodic fluid flow in an ancient subduction zone. *Journal of Geophysical Research*, **97**, 20043–20061.

—— & BYRNE, T. 1992. Strain variations in an ancient accretionary complex: implications for forearc evolution. *Tectonics*, **11**, 330–347.

GLEN, R. A. 1990. Formation and thrusting in some Great Valley rocks near the Franciscan Complex, California, and implications for the tectonic wedging hypothesis. *Tectonics*, **9**, 1451–1477.

HARMS, T., JAYKO, A. S. & BLAKE, M. C., JR 1992. Kinematic evidence for extensional unroofing of the Franciscan Complex along the Coast Range fault zone, northern Diablo Range, California. *Tectonics*, **11**, 228–241.

INGERSOLL, R. V. 1978. Paleogeography and paleotectonics of the late Mesozoic forearc basin of northern and central California. *In*: HOWELL, D. G. & MCDOUGALL, K. A. (eds) *Mesozoic Paleogeography of the Western United States*. Pacific Coast Paleogeography Symposium 2, Pacific Section, Society of Economic Paleontologists and Mineralogists, 471–482.

—— 1979. Evolution of the Late Cretaceous forearc basin, northern and central California. *Geological Society of America Bulletin*, **90**, 813–826.

JAYKO, A. S. & BLAKE, M. C., JR 1989. Deformation of the eastern Franciscan Belt, Northern California. *Journal of Structural Geology*, **11**, 375–390.

——, —— & BROTHERS, R. N. 1986. Blueschist metamorphism of the Eastern Franciscan belt, northern California. *In*: EVANS, B. W. & BROWN, E.

H. (eds) *Blueschists and Eclogites*. Geological Society of America, Memoirs, **164**, 107–124.

——, —— & HARMS, T. 1987. Attenuation of the Coast Range ophiolite by extensional faulting, and nature of the Coast Range 'thrust', California. *Tectonics*, **6**, 475–488.

KAMB, W. B. 1959. Ice petrofabric observations from Blue Glacier, Washington, in relation to theory and experiment. *Journal of Geophysical Research*, **64**, 1891–1909.

KRUEGER, S. & JONES, D. 1989. Extensional fault uplift of regional Franciscan blueschists due to subduction shallowing during the Laramide orogeny. *Geology*, **17**, 1157–1159.

KÜSTER, M. & STÖCKHERT, B. 1997. Density changes of fluid inclusions in high-pressure/low-temperature metamorphic rocks from Crete: a thermobarometric approach to the creep strength of the host minerals. *Lithos*, **41**, 151–167.

LANPHERE, M. B., BLAKE, M. C. & IRWIN, W. P. 1978. Early Cretaceous metamorphic age of the South Fork Mountain schist in the northern Coast Ranges of California. *American Journal of Science*, **278**, 798–815.

MALVERN, L. E. 1969. *Introduction to the Mechanics of a Continuum Medium*. Prentice–Hall, Englewood Cliffs, NJ.

MASSONE, H. J. & SCHREYER, W. 1987. Phengite geobarometry based on the limiting assemblage with K-feldspar, phlogopite and quartz. *Contributions to Mineralogy and Petrology*, **96**, 212–224.

MATTINSON, J. M. 1986. Geochronology of high pressure–low temperature Franciscan metabasites – a new approach using the U–Pb system. *In*: EVANS, B. W. & BROWN, E. H. (eds) *Blueschists and Eclogites*. Geological Society of America Memoir, **164**, 95–105.

—— 1988. Constraints on the timing of Franciscan metamorphism: geochronological approaches and their limitations. *In*: ERNST, W. G. (ed.) *Metamorphism and Crustal Evolution of the Western United States. Rubey Volume VII.* Prentice–Hall, Englewood Cliffs, NJ, 1023–1034.

—— & ECHEVIRRA, L. M. 1980. Ortigalita Peak gabbro, Franciscan complex – U–Pb ages of intrusion and high pressure–low temperature metamorphism. *Geology*, **8**, 589–593.

MCDOWELL, F., LEHMANN, D. H., GUCWA, P. R., FRITZ, D. & MAXWELL, J. C. 1984. Glaucophane schists and ophiolites of the northern California Coast Ranges: isotopic ages and their tectonic implications. *Geological Society of America Bulletin*, **95**, 1373–1382.

MEANS, W. D. 1994. Rotational quantities in homogeneous flow and the development of small-scale structure. *Journal of Structural Geology*, **16**, 437–445.

——, HOBBS, B. E., LISTER, G. S. & WILLIAMS, P. F. 1980. Vorticity and non-coaxiality in progressive deformation. *Journal of Structural Geology*, **5**, 279–286.

MOXON, I. W. 1988. Sequence stratigraphy of the Great Valley basin in the context of convergent margin tectonics. *In*: GRAHAM, S. A. & OLSON, H. C. (eds) *Studies of the geology of the San Joaquin Basin*. Field Trip Guidebook, Pacific Section, Society of Economic Paleontologists and Mineralogists, **60**, 3–28.

—— & GRAHAM, S. A. 1987. History and controls of subsidence in the Late Cretaceous–Tertiary Great Valley forearc basin, California. *Geological Society of America Bulletin*, **15**, 626–629.

NELSON, B. K. & DEPAOLO, D. J. 1985. Isotopic investigation of metasomatism in subduction zones – The Franciscan complex, California. *Geological Society of America Abstracts with Programs*, **17**(7), 674–675.

NORRIS, R. J. & BISHOP, D. G. 1990. Deformed conglomerates and textural zones in the Otago Schists, South Island, New Zealand. *Tectonophysics*, **174**, 331–349.

PAGE, B. M. & TABOR, L. T. 1967. Chaotic structure and décollement in Cenozoic rocks near Stanford University, California. *Geological Society of America Bulletin*, **78**, 1–12.

PAMPEYAN, E. 1993. *Geologic map of the Palo Alto and part of the Redwood Point 7–1/2' quadrangles, San Mateo and Santa Clara Counties, California*. US Geological Survey, Map **I-2371**, scale 1:24 000.

PASSCHIER, C. W. 1988. The use of Mohr circles to describe non-coaxial progressive deformation. *Tectonophysics*, **149**, 323–338.

—— 1991. The classification of dilatant flow types. *Journal of Structural Geology*, **13**, 101–104.

—— & TROUW, R. A. J. 1996. *Microtectonics*. Springer, Berlin.

PATERSON, S. R. & SAMPLE, J. C. 1988. The development of folds and cleavages in slate belts by underplating in accretionary complexes; a comparison of the Kodiak Formation, Alaska and the Calaveras Complex, California. *Tectonics*, **7**, 859–874.

—— & YU, H. 1994. Primary fabric ellipsoids in sandstones: implications for depositional processes and strain analysis. *Journal of Structural Geology*, **16**, 505–517.

PAVLIS, T. L. & BRUHN, R. L. 1983. Deep-seated flow as a mechanism for the uplift of broad forearc ridges and its role in the exposure of high *P/T* metamorphic terranes. *Tectonics*, **2**, 473–497.

PETERMAN, Z. E., HEDGE, C. E., COLEMAN, R. G. & SNAVELY, P. D., JR 1967. $^{87}Sr/^{86}Sr$ ratios in some eugeosynclinal sedimentary rocks and their bearing on the origin of granitic magma in orogenic belts. *Earth and Planetary Science Letters*, **2**, 433–439.

PLATT, J. P. 1975. Metamorphic and deformational processes in the Franciscan Complex, California: some insights from the Catalina schist terrane. *Geological Society of America Bulletin*, **86**, 1337–1347.

—— 1986. Dynamics of orogenic wedges and the uplift of high-pressure metamorphic rocks. *Geological Society of America Bulletin*, **97**, 1037–1053.

—— 1987. The uplift of high-pressure–low-temperature metamorphic rocks. *Philosophical Transactions of the Royal Society of London, Series A*, **321**, 87–103.

—— 1993. Exhumation of high-pressure rocks: a review of concepts and processes. *Terra Nova*, **5**, 119–133.

PRESS, W. H., TEUKOLSKY, S. A., VETTERLING, W. T. & FLANNERY, B. P. 1992. *Numerical Recipes in Fortran: The Art of Scientific Computing*. Cambridge University Press, Cambridge.

RAMSAY, J. G. & HUBER, M. I. 1983. *The Techniques of Modern Structural Geology, Volume 1: Strain Analysis*. Academic Press, London.

RAMTHUN, A., BRANDON, M. T. & RING, U. 1997. Fabric analysis in the Ukelayet Flysch in the footwall of the Vatyna thrust zone, Kamchatka, Russia: sedimentary or tectonic fabrics? *Terra Nova*, **9**, 377.

RING, U. 1995. Horizontal contraction or horizontal extension: heterogeneous Late Eocene and Early Oligocene general shearing during blueschist- and greenschist-facies metamorphism at the Pennine–Austroalpine boundary zone in the Western Alps. *Geologische Rundschau*, **84**, 843–859.

—— 1996. *Kinematic analysis of heterogeneous brittle deformation at the Coast Range fault zone and ductile strain and mass loss in the Eastern Franciscan belt (Franciscan subduction complex, U.S.A.): implications for the exhumation of high-pressure/low-temperature metamorphic rocks*. Habilitation thesis, Universität Mainz.

—— & BRANDON, M. T. 1994. Kinematic data for the Coast Range fault zone and implications for the exhumation of the Franciscan Subduction Complex. *Geology*, **22**, 735–738.

—— & —— 1997. Kinematics of the Coast Range fault zone, California: implications for the evolution of the Franciscan subduction complex. *Geological Society of America Abstracts with Programs*, **29**(5), 60.

——, RATSCHBACHER, L., FRISCH, W., BIEHLER, D. & KRALIK, M. 1989. Kinematics of the Alpine plate margin: structural styles, strain and motion along the Penninic–Austroalpine boundary in the Swiss–Austrian Alps. *Journal of the Geological Society, London*, **146**, 835–849.

RUBIE, D, C. 1984. A thermal–tectonic model for high-pressure metamorphism and deformation in the Sesia zone, western Alps. *Journal of Geology*, **92**, 21–36.

SELVERSTONE, J. 1985. Petrologic constraints on imbrication, metamorphism, and uplift in the SW Tauern window, Eastern Alps. *Tectonics*, **4**, 687–704.

SMITH, G. W., HOWELL, D. G. & INGERSOLL, R. V. 1979. Late Cretaceous trench-slope basins of central California. *Geology*, **7**, 303–306.

SUPPE, J. 1973. *Geology of the Leech Lake Mountain–Ball Mountain Region, California: a Cross-section of the Northeastern Franciscan Belt and its Tectonic Implications*. University of California Publications in Geological Sciences, **107**.

—— & ARMSTRONG, R. L. 1972. Potassium–argon dating of Franciscan metamorphic rocks. *American Journal of Science*, **272**, 217–233.

TAGAMI, T. & DUMITRU, T. A. 1996. Provenance and thermal history of the Franciscan accretionary complex: constraints from zircon fission track thermochronology. *Journal of Geophysical Research*, **101**, 11353–11364.

THOMSON, S. N., STÖCKHERT, B. & BRIX, M. A. 1999. Miocene high-pressure metamorphic rocks of Crete, Greece: rapid exhumation by buoyant escape. This volume.

UNRUH, J. R., LOEWEN, B. A. & MOORES, E. M. 1995. Progressive arcward contraction of a Mesozoic–Tertiary fore-arc basin, southwestern Sacramento Valley, California. *Geological Society of America Bulletin*, **107**, 38–53.

URAI, J., WILLIAMS, P. & VAN ROERMUND, H. 1991. Kinematics of crystal growth in syntectonic fibrous veins. *Journal of Structural Geology*, **13**, 823–836.

WAKABAYASHI, J. 1992. Nappes, tectonics of oblique plate convergence, and metamorphic evolution related to 140 million years of continuous subduction, Franciscan Complex, California. *Journal of Geology*, **100**, 19–40.

—— & UNRUH, J. 1995. Tectonic wedging, blueschist metamorphism, and exposure of blueschists: are they compatible? *Geology*, **23**, 85–88.

WALLIS, S., PLATT, J. & KNOTT, S. 1993. Recognition of syn-convergence extension in accretionary wedges with examples from the Calabrian Arc and the Eastern Alps. *American Journal of Science*, **293**, 463–494.

WALLIS, S. R. 1992. Vorticity analysis in a metachert from the Sanbagawa Belt, SW Japan. *Journal of Structural Geology*, **14**, 271–280.

WEINRICH, A., SHARP, W. D., RENNE, P. R. & MERTZ, D. F. 1997. Alkaline diabases in a near trench environment, Franciscan complex, California: implications from geochemical and $^{40}Ar/^{39}Ar$ data. *Terra Nova*, **9**, 352.

WENTWORTH, C. W., BLAKE, M. C., JONES, D. L., WALTER, A. W. & ZOBACK, M. D. 1984. Tectonic wedging associated with emplacement of the Franciscan assemblage, California Coast Ranges. *In*: BLAKE, M. C. (ed.) *Franciscan Geology of northern California*. Society of Economic Paleontologists and Mineralogists, Pacific Section, 163–173.

WHEELER, J. & BUTLER, R. W. H. 1994. Criteria for identifying structures related to true crustal extension in orogens. *Journal of Structural Geology*, **16**, 1023–1027.

WORRALL, D. M. 1979. *Geology of the South Yolla Bolly area, northern California and its tectonic implications*. PhD thesis, University of Texas, Austin.

—— 1981. Imbricate low-angle faulting in uppermost Franciscan rocks, South Yolla Bolly area, northern California. *Geological Society of America Bulletin*, **92**, 703–729